

InterFaceGAN: Interpreting the Disentangled Face Representation Learned by GANs

Yujun Shen, Ceyuan Yang, Xiaoou Tang, Bolei Zhou

Abstract—Although Generative Adversarial Networks (GANs) have made significant progress in face synthesis, there lacks enough understanding of what GANs have learned in the latent representation to map a randomly sampled code to a photo-realistic face image. In this work, we propose a framework, called InterFaceGAN, to interpret the disentangled face representation learned by the state-of-the-art GAN models and thoroughly analyze the properties of the facial semantics in the latent space. We first find that GANs actually learn various semantics in some linear subspaces of the latent space when being trained to synthesize high-quality faces. After identifying the subspaces of the corresponding latent semantics, we are able to realistically manipulate the facial attributes occurring in the synthesized images without retraining the model. We then conduct a detailed study on the correlation between different semantics and manage to better disentangle them via subspace projection, resulting in more precise control of the attribute manipulation. Besides manipulating gender, age, expression, and the presence of eyeglasses, we can even alter the face pose as well as fix the artifacts accidentally generated by GANs. Furthermore, we perform in-depth face identity analysis and layer-wise analysis to quantitatively evaluate the editing results. Finally, we apply our approach to real face editing by involving GAN inversion approaches as well as explicitly training additional feed-forward models based on the synthetic data established by InterFaceGAN. Extensive experimental results suggest that learning to synthesize faces spontaneously brings a disentangled and controllable face representation.

Index Terms—Generative adversarial network, face editing, interpretability, explainable artificial intelligence, disentanglement.



1 INTRODUCTION

RECENT years have witnessed the great success of Generative Adversarial Networks (GANs) [2] in high-fidelity face synthesis [1], [3], [4]. Based on adversarial training, GANs learn to map a random distribution to the real data observation and then produce photo-realistic images from randomly sampled latent codes.

Despite the appealing synthesis quality, it remains much less explored about what knowledge GANs actually learn in the latent representation and how we can reuse such knowledge to control the generation process. For example, given a latent code, how does GAN determine the facial attributes of the output face, *e.g.*, an old man or a young woman? How are different attributes organized in the latent space and are they entangled or disentangled? Can we manipulate the attributes of the synthesized face as we want? How does the attribute manipulation affect the face identity? Can we apply a well-trained GAN model for real image editing?

To answer these questions, we propose a novel framework, termed as *InterFaceGAN*, to *Interpret* the latent *Face* representation learned by GAN models. For this purpose, we employ some off-the-shelf classifiers to predict semantic scores for the images synthesized by GANs. In this way, we are able to bridge the latent space and the semantic space and further utilize such connection for representation analysis. In particular, we analyze how an individual semantic is encoded in the latent space *both theoretically and*

empirically. It turns out that a true-or-false facial attribute actually aligns with a linear subspace of the latent space. Based on this discovery, we study the entanglement between different semantics emerging in the latent representation and manage to disentangle them via subspace projection.

Besides finding the latent semantics, InterFaceGAN proposes an effective pipeline for face editing. By simply modulating the latent code, we can successfully manipulate the gender, age, expression, presence of eyeglasses, and even facial pose of the synthesized image, as shown in Fig.1(a). In addition, thanks to our disentanglement analysis, we propose conditional manipulation to alter one attribute without affecting others, as shown in Fig.1(b). More importantly, InterFaceGAN achieves high-quality face manipulation by reusing the semantic knowledge learned by GANs *without* any retraining.

To get a better interpretation of the semantics in the GAN representation, we conduct thorough analysis on the editing results made by InterFaceGAN. First, we compare the semantic scores before and after the manipulation to quantitatively verify whether the semantics identified by InterFaceGAN are indeed manipulable. Then, we make layer-wise analysis on StyleGAN, whose generator is with per-layer stochasticity [3], to explore how semantics originate from the latent representation layer by layer. Finally, considering the importance of the identity information for faces, we make in-depth identity analysis to see how identity is preserved in the manipulation process as well as how identity is sensitive to different facial attributes.

How to apply a GAN model to real image editing is another important issue since GANs commonly lack the inference ability. In this work, we integrate two approaches to extend InterFaceGAN to real face manipulation. One is

• Y. Shen, C. Yang, X. Tang, and B. Zhou are with the Department of Information Engineering, the Chinese University of Hong Kong, Hong Kong SAR, China.
E-mail: {sy116, yc019, xtang, bzhou}@ie.cuhk.edu.hk

Code and models are available at <https://genforce.github.io/interfacegan/>.

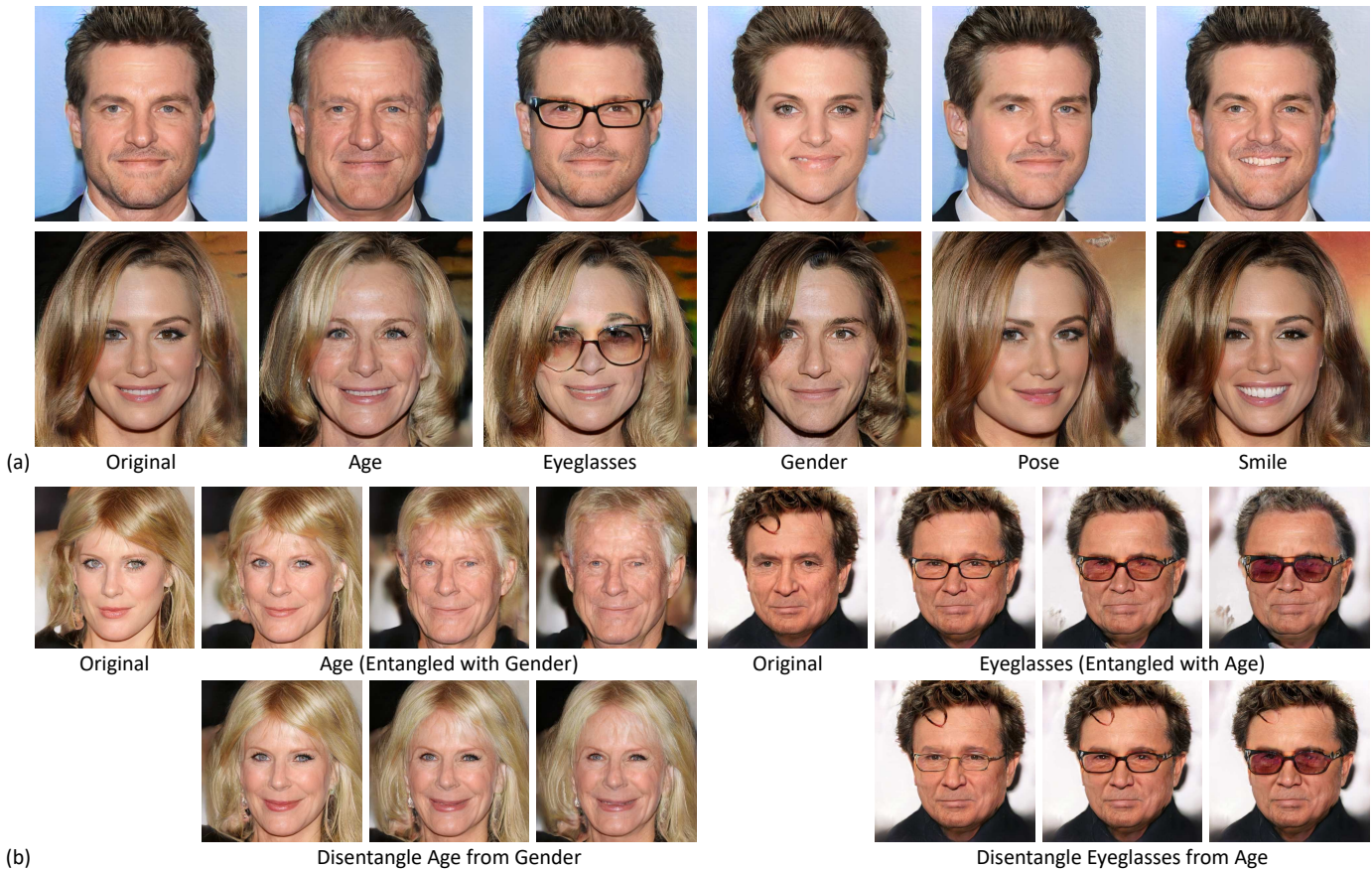


Fig. 1. (a) **Manipulating various facial attributes** through varying the latent codes of a well-trained GAN model. (b) **Conditional manipulation** results using InterFaceGAN, where we can better disentangle the correlated attributes (top row) and achieve more precise control of the facial attributes (bottom row). All results are synthesized by PGGAN [1].

to combine with GAN inversion, which is able to invert a target image back to a latent code, and then directly vary the inverted code. The other is to use InterFaceGAN to build a synthetic dataset which contains the pairs of synthetic images before and after manipulation and then train a pixel-to-pixel model on this dataset. We compare these approaches and evaluate their strengths and weaknesses.

The preliminary result of this work is published at [5]. Compared to the previous conference paper, we include following new contents: (i) a detailed analysis on the face representation learned by StyleGAN [3] as well as its comparison to the representation learned by PGGAN [1]; (ii) a comparison between the entanglement of latent semantics and the attribute distribution of training data, which sheds light on how GANs learn to encode various semantics during the training process; (iii) quantitative evaluation on the editing results achieved by InterFaceGAN; (iv) layer-wise analysis on the per-layer representation learned by StyleGAN [3]; (v) identity analysis on the images before and after manipulation; and (vi) a new method to apply InterFaceGAN to real face editing, which is to train feed-forward models on the synthetic data collected by InterFaceGAN.

2 RELATED WORK

Generative Adversarial Networks. Due to the great potential of GAN [2] in producing photo-realistic images, it

has been widely applied to image editing [6], [7], super-resolution [8], [9], image inpainting [10], [11], video synthesis [12], [13], *etc.* Many attempts have been made to improve GANs by introducing new criteria [14], [15], [16], designing novel network structures [3], [17], [18], or optimizing the training pipeline [1], [19]. The recent StyleGAN2 [4] model achieves state-of-the-art face synthesis results with incredible image quality. Despite this tremendous success, little work has been done on understanding how GANs learn to connect the latent representation with the semantics in the real visual world.

Study on Latent Space of GANs. Latent space of GANs is generally treated as Riemannian manifold [20], [21], [22]. Prior work focused on exploring how to make the output image vary smoothly from one synthesis to another through interpolation in the latent space [23], [24]. Bojanowski *et al.* [25] optimized the generator and latent code simultaneously to learn a better representation. However, the studies on how a well-trained GAN is able to encode different semantics in the latent space as well as how to reuse these semantic knowledge to control the generation process are still missing. Bau *et al.* [26] found that some units from intermediate layers of the GAN generator are specialized to synthesize certain visual concepts, such as sofa and TV for living room synthesis. Some work [27], [28] observed the vector arithmetic property in the latent space. Beyond that, this work provides detailed analysis on how semantics are encoded in the face representation

learned by GANs from both the property of a single semantic and the disentanglement of multiple semantics. Some concurrent work also explores the latent semantics in GANs: Goetschalckx *et al.* [29] improves the memorability of the output image. Jahanian *et al.* [30] studies the steerability of GANs concerning camera motion and image color tone. Yang *et al.* [31] observes the semantic hierarchy emerging in the scene synthesis models. Unlike them, we focus on interpreting the face representation by theoretically and empirically studying how various semantics originate from and are organized in the latent space. We further extend our method to *real image* editing.

Semantic Face Editing with GANs. Semantic face editing aims at manipulating facial attributes of a given image. Compared to unconditional GANs which can generate image arbitrarily, semantic editing expects the model to only change the target attribute but maintain other information of the input face. To achieve this goal, current methods required carefully designed loss functions [32], [33], [34], introduction of additional attribute labels [6], [35], [36], [37], [38], or special architectures [39], [40] to train new models. Different from previous learning-based methods, this work explores the interpretable semantics inside the latent space of *fixed* GAN models. By reusing the semantic knowledge spontaneously learned by GANs, we are able to unleash its manipulation capability and *turn unconstrained GANs to controllable GANs* by simply varying the latent code.

GAN Inversion. GAN is typically formulated as a two-player game, where a generator takes a sampled latent code as the input and outputs an image synthesis while a discriminator differentiates real domain from synthesized domain. Hence, it leaves no space for making inference on real images. To enable real image editing with fixed GAN models [7], [41], a common practice is to get the reverse mapping from the image space to the latent space, which is also known as GAN Inversion [42], [43], [44]. Prior work either performed instance-level optimization [45], [46], [47] or explicitly learned an encoder corresponding to the generator [48], [49], [50]. Some methods combined these two ideas by using the encoder to produce a good starting point for optimization [51], [52]. Recently, the GAN inversion task is significantly advanced: Gu *et al.* [53] proposes to increase the number of latent codes for a better image reconstruction. Pan *et al.* [54] optimizes the latent code together with the model weights. Zhu *et al.* [55] takes semantic information into account besides recovering the pixel values. Being orthogonal to these approaches, our work interprets the representation learned by GANs and then utilizes GAN inversion as a tool to enable real image editing by reusing the latent knowledge.

Image-to-Image Translation. Image-to-Image translation, aiming at learning a deterministic model to transfer images from one domain to another, is another way to manipulate real images. Existing work used image-to-image translation models to generate photo-realistic images from scene layouts [56], [57], sketches [58], or segmentation labels [59]. This idea is further freed from the requirement of paired training data, resulting in an unsupervised learning manner [60], [61]. There are also some attempts that increase the diversity of the translated images by introducing

stochasticity [62], [63] or translate images among multiple domains [64], [65]. However, all these models rely on paired data or domain labels, which are not that easy to obtain. In this work, we manage to leverage the semantics learned by GANs to create unlimited synthetic data pairs. By training image-to-image translation networks with such synthetic data, we are able to apply the knowledge encoded in the latent representation to feed-forward real image editing.

3 FRAMEWORK OF INTERFACEGAN

In this section, we introduce the framework of InterfaceGAN. We first provide rigorous analysis on several properties of the semantic attributes emerging in the latent space of well-trained GAN models, and then construct a pipeline of utilizing the identified semantics in latent code for face editing.

3.1 Semantics in Latent Space

Given a well-trained GAN model, the generator can be formulated as a deterministic function $g : \mathcal{Z} \rightarrow \mathcal{X}$. Here, $\mathcal{Z} \subseteq \mathbb{R}^d$ denotes the d -dimensional latent space, for which Gaussian distribution $\mathcal{N}(\mathbf{0}, \mathbf{I}_d)$ is commonly used [1], [3], [16], [19]. \mathcal{X} stands for the image space, where each sample \mathbf{x} possesses certain semantic information, like gender and age for face model. Suppose we have a semantic scoring function $f_S : \mathcal{X} \rightarrow \mathcal{S}$, where $\mathcal{S} \subseteq \mathbb{R}^m$ represents the semantic space with m semantics. We can bridge the latent space \mathcal{Z} and the semantic space \mathcal{S} with $\mathbf{s} = f_S(g(\mathbf{z}))$, where \mathbf{s} and \mathbf{z} denote semantic scores and the sampled latent code respectively.

Single Semantic. It has been widely observed that when linearly interpolating two latent codes \mathbf{z}_1 and \mathbf{z}_2 , the appearance of the corresponding synthesis changes continuously [3], [19], [27]. It implicitly means that the semantics contained in the image also change gradually. According to *Property 1*, the linear interpolation between \mathbf{z}_1 and \mathbf{z}_2 forms a direction in \mathcal{Z} , which further defines a hyperplane. We therefore make an assumption¹ that for any binary semantic (e.g., male *v.s.* female), there exists a hyperplane in the latent space serving as the separation boundary. Semantic remains the same when the latent code walks within one side of the hyperplane yet turns into the opposite when across the boundary.

Given a hyperplane with unit normal vector $\mathbf{n} \in \mathbb{R}^d$, we define the “distance” from a sample \mathbf{z} to this hyperplane as

$$d(\mathbf{n}, \mathbf{z}) = \mathbf{n}^T \mathbf{z}. \quad (1)$$

Here, $d(\cdot, \cdot)$ is not a strictly defined distance since it can be negative. When \mathbf{z} lies near the boundary and is moved toward and across the hyperplane, both the “distance” and the semantic score vary accordingly. And it is just at the time when the “distance” changes its numerical sign that the semantic attribute reverses. We therefore expect these two to be linearly dependent with

$$f(g(\mathbf{z})) = \lambda d(\mathbf{n}, \mathbf{z}), \quad (2)$$

where $f(\cdot)$ is the scoring function for a particular semantic, and $\lambda > 0$ is a scalar to measure how fast the semantic varies

1. This assumption is empirically demonstrated in Sec.4.

along with the change of “distance”. According to *Property 2*, random samples drawn from $\mathcal{N}(\mathbf{0}, \mathbf{I}_d)$ are very likely to locate close enough to a given hyperplane. Therefore, the corresponding semantic can be modeled by the linear subspace that is defined by \mathbf{n} .

Property 1 Given $\mathbf{n} \in \mathbb{R}^d$ with $\mathbf{n} \neq \mathbf{0}$, the set $\{\mathbf{z} \in \mathbb{R}^d : \mathbf{n}^T \mathbf{z} = 0\}$ defines a hyperplane in \mathbb{R}^d , and \mathbf{n} is called the normal vector. All vectors $\mathbf{z} \in \mathbb{R}^d$ satisfying $\mathbf{n}^T \mathbf{z} > 0$ locate from the same side of the hyperplane.

Property 2 Given $\mathbf{n} \in \mathbb{R}^d$ with $\mathbf{n}^T \mathbf{n} = 1$, which defines a hyperplane, and a multivariate random variable $\mathbf{z} \sim \mathcal{N}(\mathbf{0}, \mathbf{I}_d)$, we have $P(|\mathbf{n}^T \mathbf{z}| \leq 2\alpha \sqrt{\frac{d}{d-2}}) \geq (1 - 3e^{-cd})(1 - \frac{2}{\alpha} e^{-\alpha^2/2})$ for any $\alpha \geq 1$ and $d \geq 4$. Here, $P(\cdot)$ stands for probability and c is a fixed positive constant.²

Multiple Semantics. When the case comes to m different semantics, we have

$$\mathbf{s} \equiv f_S(g(\mathbf{z})) = \Lambda \mathbf{N}^T \mathbf{z}, \quad (3)$$

where $\mathbf{s} = [s_1, \dots, s_m]^T$ denotes the semantic scores, $\Lambda = \text{diag}(\lambda_1, \dots, \lambda_m)$ is a diagonal matrix containing the linear coefficients, and $\mathbf{N} = [\mathbf{n}_1, \dots, \mathbf{n}_m]$ indicates the separation boundaries. Aware of the distribution of random sample \mathbf{z} , which is $\mathcal{N}(\mathbf{0}, \mathbf{I}_d)$, we can easily compute the mean and covariance matrix of the semantic scores \mathbf{s} as

$$\boldsymbol{\mu}_s = \mathbb{E}(\Lambda \mathbf{N}^T \mathbf{z}) = \Lambda \mathbf{N}^T \mathbb{E}(\mathbf{z}) = \mathbf{0}, \quad (4)$$

$$\begin{aligned} \boldsymbol{\Sigma}_s &= \mathbb{E}(\Lambda \mathbf{N}^T \mathbf{z} \mathbf{z}^T \mathbf{N} \Lambda^T) = \Lambda \mathbf{N}^T \mathbb{E}(\mathbf{z} \mathbf{z}^T) \mathbf{N} \Lambda^T \\ &= \Lambda \mathbf{N}^T \mathbf{N} \Lambda. \end{aligned} \quad (5)$$

We therefore have $\mathbf{s} \sim \mathcal{N}(\mathbf{0}, \boldsymbol{\Sigma}_s)$, which is a multivariate normal distribution. Different entries of \mathbf{s} are disentangled if and only if $\boldsymbol{\Sigma}_s$ is a diagonal matrix, which requires $\{\mathbf{n}_1, \dots, \mathbf{n}_m\}$ to be orthogonal with each other. If this condition does not hold, some semantics will entangle with each other. $\mathbf{n}_i^T \mathbf{n}_j$ can be used to measure the entanglement between the i -th and j -th semantics to some extent.

3.2 Manipulation in Latent Space

In this part, we introduce how to use the semantics found in the latent space for image editing.

Single Attribute Manipulation. According to Eq.(2), to manipulate the attribute of a synthesized image, we can easily edit the original latent code \mathbf{z} with $\mathbf{z}_{edit} = \mathbf{z} + \alpha \mathbf{n}$. It will make the synthesis look more positive on such semantic with $\alpha > 0$ since the score becomes $f(g(\mathbf{z}_{edit})) = f(g(\mathbf{z})) + \lambda \alpha$ after editing. Similarly, $\alpha < 0$ will make the synthesis look more negative.

Conditional Manipulation. When there is more than one attribute, editing one may affect another since some semantics can be coupled with each other. To achieve more precise control, we propose *conditional manipulation* by manually forcing $\mathbf{N}^T \mathbf{N}$ in Eq.(5) to be diagonal. In particular, we use projection to orthogonalize different vectors. As shown in Fig.2, given two hyperplanes with normal vectors \mathbf{n}_1 and \mathbf{n}_2 , we find a projected direction $\mathbf{n}_1 - (\mathbf{n}_1^T \mathbf{n}_2) \mathbf{n}_2$, such that moving samples along this new direction can change

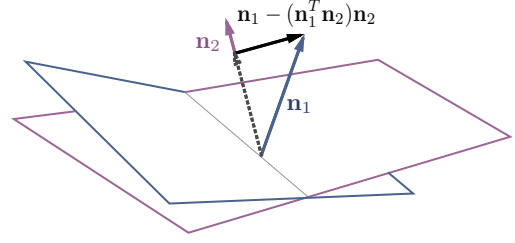


Fig. 2. Illustration of the **conditional manipulation via subspace projection**. The projection of \mathbf{n}_1 onto \mathbf{n}_2 is subtracted from \mathbf{n}_1 , resulting in a new direction $\mathbf{n}_1 - (\mathbf{n}_1^T \mathbf{n}_2) \mathbf{n}_2$.

“attribute 1” without affecting “attribute 2”. If there are multiple attributes to be conditioned on, we just subtract the projection from the primal direction onto the plane that is constructed by all conditioned directions.

Real Image Manipulation. InterFaceGAN enables semantic editing from the latent space of a *fixed* GAN model. Therefore, to manipulate real images, a straightforward way is to infer the best latent code that can be used to reconstruct the target image, *i.e.*, GAN inversion. For this purpose, both optimization-based [55] and learning-based [50] approaches can be used. We thoroughly evaluate their strengths and weaknesses in Sec.6. We also use InterFaceGAN to prepare synthetic data pairs and then train image-to-image translation models [59] to achieve real face editing. This kind of approach is also analyzed in Sec.6.

3.3 Implementation Details

We choose five key facial attributes for analysis, including pose, smile (expression), age, gender, and eyeglasses. The corresponding positive directions are defined as turning right, laughing, getting old, changing to male, and wearing eyeglasses. Note that we can always easily plug in more attributes as long as the attribute predictor (scoring function) is available.

To better predict these attributes from synthesized images, we train an auxiliary attribute prediction model using the annotations from the CelebA dataset [66] with ResNet-50 network [67]. This model is trained with multi-task losses to simultaneously predict smile, age, gender, eyeglasses, as well as the 5-point facial landmarks (left eye, right eye, nose, left corner of mouth, right corner of mouth). Here, the facial landmarks are used to compute yaw pose, which is also treated as a binary attribute (left or right) in further analysis. Besides the landmarks, all other attributes are learned as a bi-classification problem with softmax cross-entropy loss, while landmarks are optimized with l_2 regression loss. As images produced by PGGAN and StyleGAN are with 1024×1024 resolution, we resize them to 224×224 before feeding them to the attribute model.

Given the pre-trained GAN model, we synthesize 500K images by randomly sampling from the latent space. There are mainly two reasons in preparing such large-scale dataset: (i) to eliminate the randomness caused by sampling and make sure the distribution of the sampled code is as expected, and (ii) to get enough wearing-glasses samples, which are really rare in PGGAN model.

To find the semantic boundaries in latent space, we use the pre-trained attribute prediction model to assign

². When $d = 512$, we have $P(|\mathbf{n}^T \mathbf{z}| > 5.0) < 1e^{-6}$. It suggests that almost all sampled latent codes are expected to locate within 5 unit-length to the boundary. Proof can be found in **Appendix**.

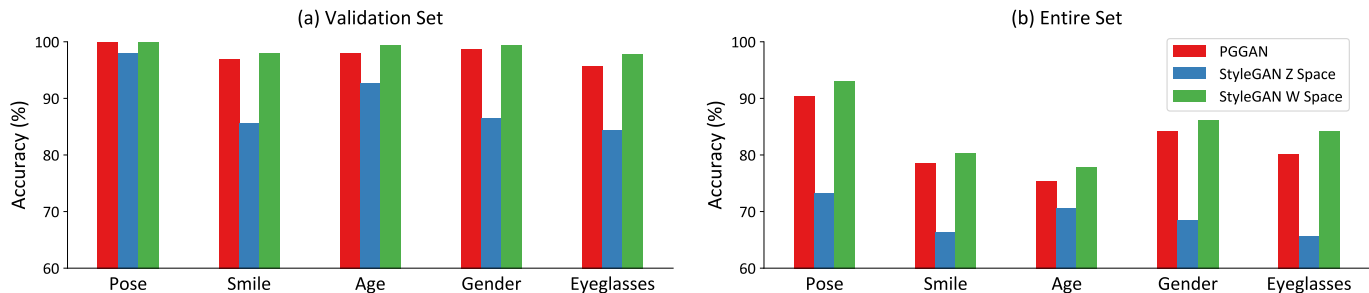


Fig. 3. Classification accuracy (%) on the latent separation boundaries of PGGAN [1] and StyleGAN [3] with respect to different attributes.

attribute scores for all 500K synthesized images. For each attribute, we sort the corresponding scores and choose 10K samples with the highest scores and 10K with the lowest ones as candidates. The reason in doing so is that the prediction model is not absolutely accurate and may produce wrong predictions for ambiguous samples, *e.g.*, middle-aged person for age attribute. We then randomly choose 70% samples from the candidates as the training set to learn a linear SVM, resulting in a decision boundary. Recall that, normal directions of all boundaries are normalized to unit vectors. Remaining 30% samples are used for verifying how the linear classifier behaves. Here, for SVM training, the inputs are the 512d latent codes, while the binary labels are assigned by the auxiliary attribute prediction model.

4 INTERPRETING FACE REPRESENTATION

In this section, we apply InterFaceGAN to interpreting the face representation learned by state-of-the-art GAN models, *i.e.*, PGGAN [1] and StyleGAN [3], both of what are able to produce high-quality faces with 1024×1024 resolution. PGGAN is a representative of traditional generator where the latent code is only fed into the very first convolutional layer. By contrast, StyleGAN proposed a style-based generator, which first maps the latent code from latent space \mathcal{Z} to a disentangled latent space \mathcal{W} before applying it for generation. In addition, the disentangled latent code is fed to all convolutional layers.

4.1 Separability of Latent Space

As mentioned in Sec.3.1, our framework is based on an assumption that for any binary attribute, there exists a hyperplane in the latent space such that all samples from the same side are with the same attribute. In this part, we would like to first evaluate the correctness of this assumption to make the remaining analysis considerable.

4.1.1 PGGAN

For each attribute, we will get a latent boundary after the training of the linear SVM classifier. We evaluate the classification performance on the validation set (3K positive testing samples and 3K negative testing samples) as well as the entire set (remaining 480K samples besides the 20K candidates with high confidence level). Fig.3 shows the results. We find that all linear boundaries of PGGAN achieve over 95% accuracy on the validation set and over 75% on the entire set, suggesting that for a binary attribute,

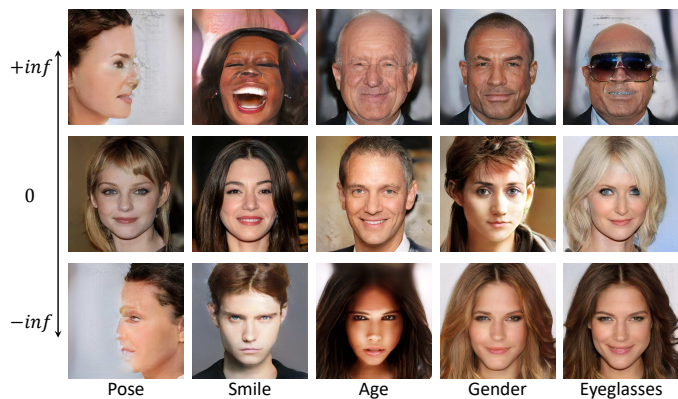


Fig. 4. Synthesized samples by PGGAN [1] with the distance near to (middle row) and extremely far away from (top and bottom rows) the separation boundary. Each column corresponds to a particular attribute.

there indeed exists a linear hyperplane in the latent space that can well separate the data into two groups.

We also visualize some samples in Fig.4 through ranking them by the “distance” to the decision boundary. Note that those extreme cases (top and bottom rows) are very unlikely to be directly sampled, instead constructed by moving a latent code towards the normal direction “infinitely”. From Fig.4, we can tell that the positive samples and negative samples are distinguishable to each other with respect to the corresponding attribute. This further demonstrates that the latent space is linearly separable and InterFaceGAN is able to successfully find the proper separation hyperplane.

4.1.2 StyleGAN

Compared to PGGAN, StyleGAN employs two latent spaces, which are the native latent space \mathcal{Z} and the mapped latent space \mathcal{W} . We analyze the separability of both spaces and the results are shown in Fig.3. Note that \mathcal{W} space is not subject to normal distribution like \mathcal{Z} space, but we can conduct a similar analysis on \mathcal{W} space, demonstrating the generalization ability of InterFaceGAN.

We mainly have three observations from Fig.3. (i) Boundaries from both \mathcal{Z} space and \mathcal{W} space separate the validation set well. Even though the performances of \mathcal{Z} boundaries on the entire set are not satisfying, it may be caused by the inaccurate attribute prediction on the ambiguous samples. (ii) \mathcal{W} space shows much stronger separability than \mathcal{Z} space. That is because $\mathbf{w} \in \mathcal{W}$, instead of $\mathbf{z} \in \mathcal{Z}$, is the code finally fed into the generator. Accordingly, the generator tends to learn various semantics based on \mathcal{W} space. (iii) The accuracy of StyleGAN \mathcal{W} space is higher than the PGGAN

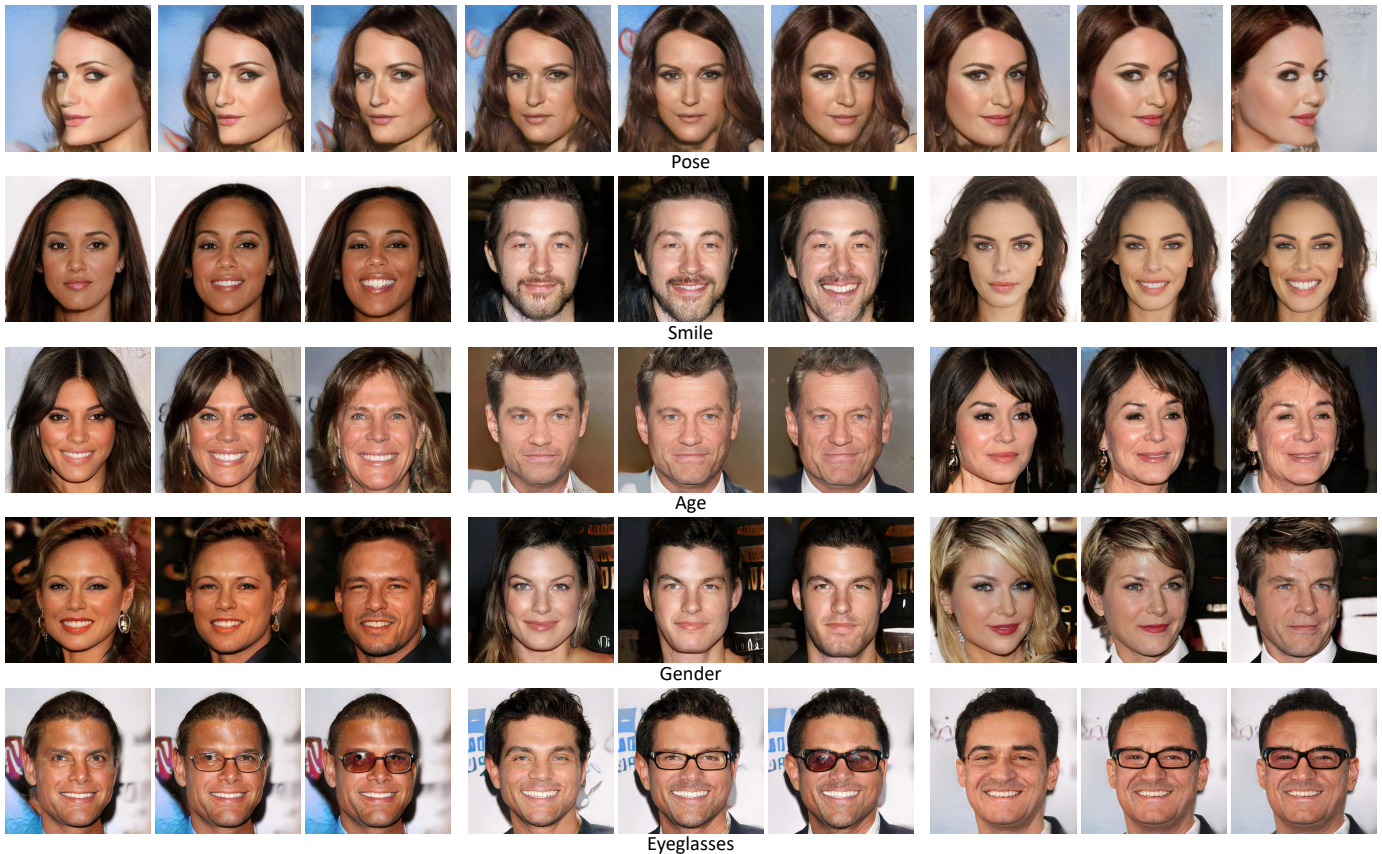


Fig. 5. **Single attribute manipulation** results with PGGAN [1]. The first row shows the same person under gradually changed poses. The following rows correspond to the results of manipulating four different attributes. For each set of three samples in a row, the central one is the original synthesis, while the left and right stand for the results by moving the latent code in negative and positive directions respectively.



Fig. 6. Illustration of the **distance effect** by taking gender manipulation with PGGAN [1] as an example. The image in the red dashed box stands for the original synthesis. Our approach performs well when the latent code locates close to the boundary. However, when the distance keeps increasing, the synthesized images are no longer like the same person.



Fig. 7. Examples on **fixing the artifacts** that PGGAN [1] has generated. First row shows some bad generation results, while the following two rows present the gradually corrected synthesis by moving the latent codes along the positive “quality” direction.

\mathcal{Z} space, both of which are the immediate input space of the generator. The reason is that the semantic attributes may not be normally distributed in real data. Compared to \mathcal{Z} space, which is subject to normal distribution, \mathcal{W} space has no constraints and hence is able to better fit the underlying real distribution.

4.2 Semantics in Latent Space for Face Manipulation

In this part, we verify whether the semantics found by InterFaceGAN are manipulable.

4.2.1 PGGAN

Manipulating Single Attribute. Fig.5 plots the manipulation results on five different attributes. It suggests that our manipulation approach performs well on all attributes in both positive and negative directions. Particularly on *pose* attribute, we observe that even the boundary is searched by solving a bi-classification problem, moving the latent code can produce continuous changing. Furthermore, although

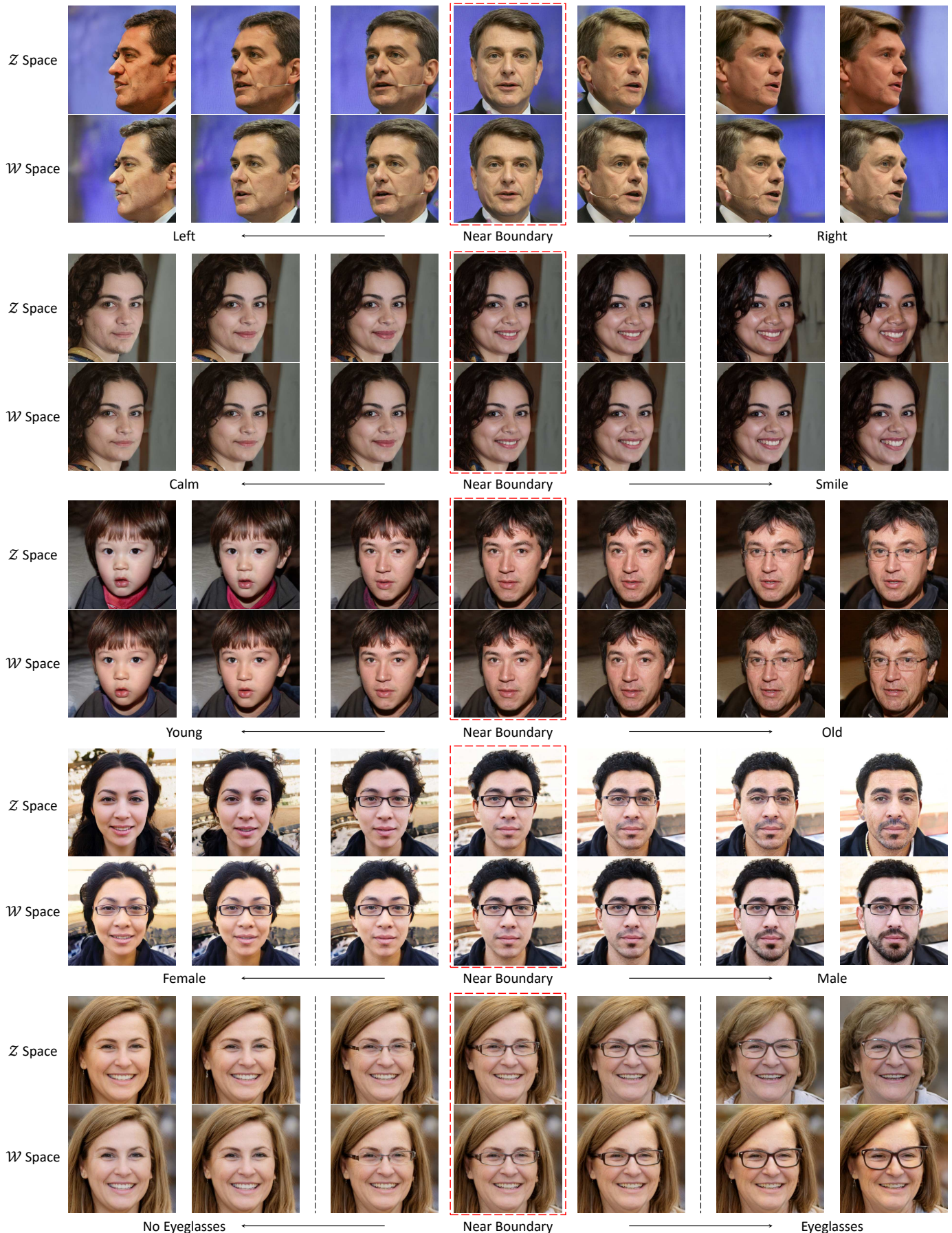


Fig. 8. **Attribute editing** results on StyleGAN [3]. For each attribute, top row shows the manipulation results with respect to \mathcal{Z} space, whilst bottom row corresponds to \mathcal{W} space. Images in red dashed boxes represent the original synthesis. Images between two black dashed lines stand for near-boundary manipulation, and other images stand for long-distance manipulation.

TABLE 1
Disentanglement analysis on PGGAN [1].

(a) Training data.						(b) Synthesized data.						(c) Semantic boundaries.					
	Pose	Smile	Age	Gender	Glasses		Pose	Smile	Age	Gender	Glasses		Pose	Smile	Age	Gender	Glasses
Pose	1.00	-0.01	0.00	0.00	0.01	Pose	1.00	-0.01	-0.01	-0.02	0.00	Pose	1.00	-0.04	-0.06	-0.05	-0.04
Smile		1.00	0.03	-0.09	-0.03	Smile		1.00	0.02	-0.08	-0.01	Smile		1.00	0.04	-0.10	-0.05
Age			1.00	0.20	0.15	Age			1.00	0.42	0.35	Age			1.00	0.49	0.38
Gender				1.00	0.19	Gender				1.00	0.47	Gender				1.00	0.52
Glasses					1.00	Glasses					1.00	Glasses					1.00

there lacks enough data with extreme poses in the training set, GAN is capable of imagining how profile faces should look like. The same situation also happens on eyeglasses attribute. We can manually create a lot of faces wearing eyeglasses despite the inadequate data in the training set. These two observations provide strong evidence that GAN does not produce images randomly, but learns some interpretable semantics in the latent space.

Distance Effect of Semantic Subspace. When manipulating the latent code, we observe an interesting distance effect, which is that the samples will suffer from severe changes in appearance if being moved too far from the boundary, and finally tend to become the extreme cases shown in Fig.4. Fig.6 illustrates this phenomenon by taking gender editing as an instance. Near-boundary manipulation works well. When samples go beyond a certain region³, however, the editing results are no longer like the original face anymore. But this effect does not affect our understanding of the disentangled semantics in the latent space. That is because such extreme samples are very unlikely to be directly drawn from a standard normal distribution, which is pointed out in *Property 2* in Sec.3.1. Instead, they are constructed manually by keeping moving a normally sampled latent code along a certain direction.

Artifacts Correction. We further apply our approach to fix the artifacts that sometimes occurring in the synthesis. We manually labeled 4K bad synthesis and then trained a linear SVM to find the separation hyperplane, same as other attributes. We surprisingly find that GAN also encodes such quality information in the latent space. Based on this discovery, we manage to correct some mistakes GAN has made in the generation process by moving the latent code towards the positive “quality” direction, as shown in Fig.7.

4.2.2 StyleGAN

We further apply InterFaceGAN to StyleGAN model by manipulating the latent codes in both \mathcal{Z} space and \mathcal{W} space. We have the following observations from Fig.8. (i) Besides the conventional generator (e.g., PGGAN), InterFaceGAN all works well on the style-based generator. We can successfully edit the attributes by moving the latent code along the corresponding directions in either \mathcal{Z} space or \mathcal{W} space. (ii) By learning from a more diverse dataset, FF-HQ [3], StyleGAN learns various semantics more thoroughly. For example, StyleGAN can even generate children when making people younger (third example). This is beyond the ability of PGGAN, which is trained on CelebA-HQ [1].

3. We choose 5.0 as the threshold.

Also, StyleGAN is capable of producing faces with extreme poses. (iii) \mathcal{W} space shows better performance than \mathcal{Z} space, especially for long-distance manipulation. In other words, when the latent code locates near the separation boundary (between the two dashed lines), manipulations in \mathcal{Z} space and \mathcal{W} space have similar effect. However, when the latent code goes further from the boundary, manipulating one attribute in \mathcal{Z} space might affect another. Taking gender editing (fourth example) as an instance, the person in the red box takes off his eyeglasses when moving along the gender direction. By contrast, \mathcal{W} space shows stronger robustness. (iv) Some attributes are correlated to each other. For example, people are wearing eyeglasses when turning old (third example), and people are tending to become happier when being feminized (fourth example). More detailed analysis about this phenomenon will be discussed in Sec.4.3.

4.3 Disentanglement Analysis and Conditional Manipulation

In this section, we study the disentanglement between different semantics encoded in the latent representation and evaluate the conditional manipulation approach.

4.3.1 Disentanglement Measurement

Different from Karras *et al.* [3] which introduced perceptual path length and linear separability to measure the disentanglement property of the latent space, we focus more on the relationship between different attributes and study how they are entangled with each other. In other words, besides the problem that how one semantic can be well encoded in the latent space, we also explore the correlations between multiple semantics and try to decouple them. In particular, we use following metrics for analysis.

- 1) *Attribute correlation of real data.* We use the prepared predictors to predict the attribute scores of real data on which the GAN model is trained. Then we compute the correlation coefficient ρ between any two attributes with $\rho_{A_1, A_2} = \frac{Cov(A_1, A_2)}{\sigma_{A_1} \sigma_{A_2}}$. Here, A_1 and A_2 represent two random variables with respect to these two attributes. $Cov(\cdot, \cdot)$ and σ denote covariance and standard deviation respectively.
- 2) *Attribute correlation of synthesized data.* We also compute the attribute correlation score on the 500K synthesized data. By comparing this score to that of the real data, we can get some clues on how GANs learn to encode such semantic knowledge in the latent representation.

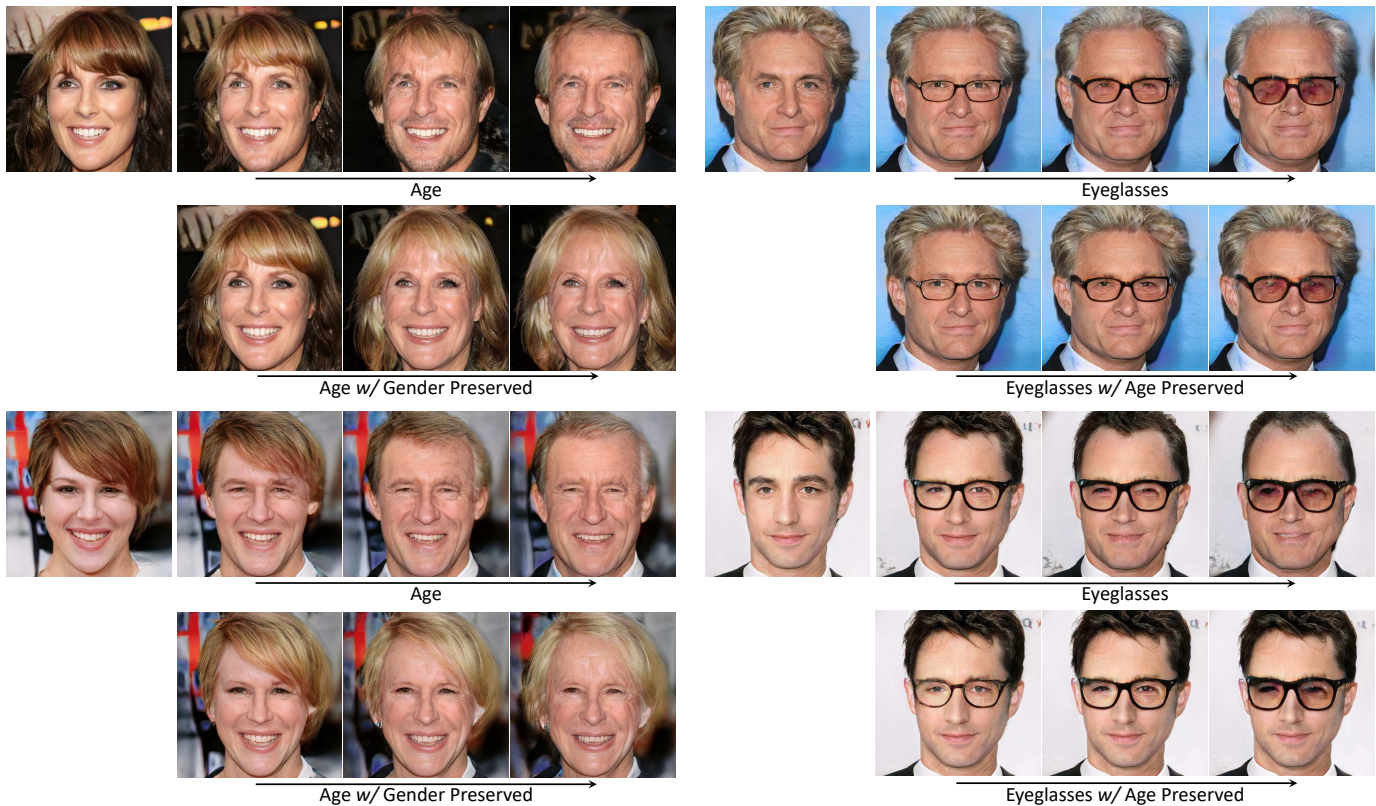


Fig. 9. **Conditional manipulation** results using PGGAN [1]. Left: Manipulating age attribute by keeping gender maintained. Right: Manipulating eyeglasses attribute by keeping age maintained. For each example, top row shows the unconditional editing results while bottom shows the conditional manipulation.

- 3) *Semantic boundary correlation*. Given any two semantics, with the latent boundaries \mathbf{n}_1 and \mathbf{n}_2 , we compute the cosine similarity between these two directions with $\cos(\mathbf{n}_1, \mathbf{n}_2) = \mathbf{n}_1^T \mathbf{n}_2$. Here, \mathbf{n}_1 and \mathbf{n}_2 are both unit vectors. This metric is used to evaluate how the above attribute correlation is reflected in our InterFaceGAN framework.

4.3.2 PGGAN

Disentanglement Analysis. Tab.1 reports the correlation metrics of PGGAN model trained on CelebA-HQ dataset [1]. By comparing the attribution correlation of real data (Tab.1(a)) and that of synthesized data (Tab.1(b)), we can tell that they are very close to each other. For example, “pose” and “smile” are almost independent to other attributes, while “gender”, “age”, and “eyeglasses” are highly correlated with each other from both real data and synthesized data, which means old men are more likely to wear eyeglasses. This implies that GANs actually learn the underlying semantic distribution from the real observation when trained to synthesize images. Then, by comparing such attribution correlation with the boundary correlation (Tab.1(c)), we also find that they behave similarly. This suggests that InterFaceGAN is able to not only accurately identify the semantics encoded in that latent representation but also capture the entanglement among them.

Conditional Manipulation. As shown in Tab.1(c), if two boundary are not orthogonal to each other, modulating the latent code along one direction will definitely affect

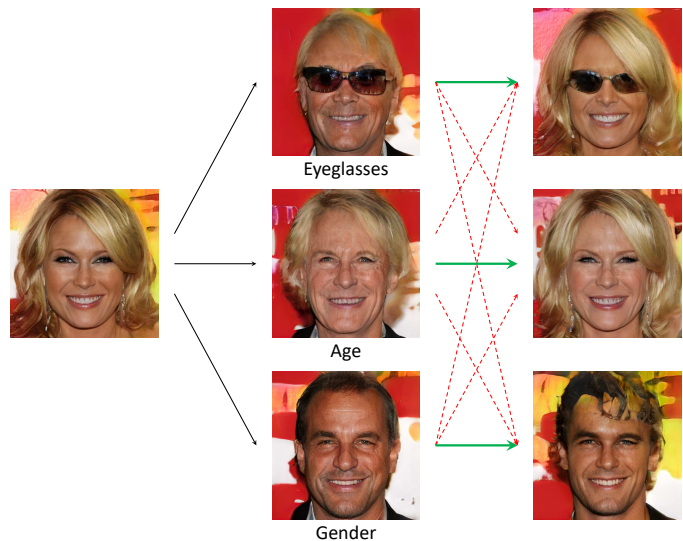


Fig. 10. **Conditional manipulation results with more than one conditions** using PGGAN [1]. Left: Original synthesis. Middle: Manipulations along single boundary. Right: Conditional manipulations. Green arrows indicate the primal direction and red arrows represent the directions to condition on.

the other. Hence, we propose conditional manipulation via subspace projection to eliminate this entanglement as much as possible. Details are described in Sec.3.2. Fig.9 shows the discrepancies between unconditional manipulation and conditional manipulation. Taking the top-left example in Fig.9 as an instance, the results tend to become male when being edited to get old (top row). We fix this problem by

TABLE 2
Disentanglement analysis on StyleGAN [3].

(a) Training data.						(b) Synthesized data.					
Pose	Pose	Smile	Age	Gender	Glasses	Pose	Pose	Smile	Age	Gender	Glasses
Smile	1.00	-0.02	0.00	-0.02	-0.01	Smile	1.00	1.00	0.01	0.00	-0.01
Age		1.00	0.01	-0.17	-0.03	Age			1.00	-0.22	-0.02
Gender			1.00	0.14	0.21	Gender				1.00	0.45
Glasses				1.00	0.20	Glasses					1.00
					1.00						1.00

(c) Semantic boundaries from \mathcal{Z} space.						(d) Semantic boundaries from \mathcal{W} space.					
Pose	Pose	Smile	Age	Gender	Glasses	Pose	Pose	Smile	Age	Gender	Glasses
Smile	1.00	-0.03	0.03	-0.01	-0.08	Smile	1.00	0.00	0.02	0.03	-0.03
Age		1.00	-0.28	-0.42	-0.20	Age		1.00	0.03	-0.06	0.02
Gender			1.00	0.33	0.72	Gender			1.00	0.07	0.05
Glasses				1.00	0.44	Glasses				1.00	0.00
					1.00						1.00

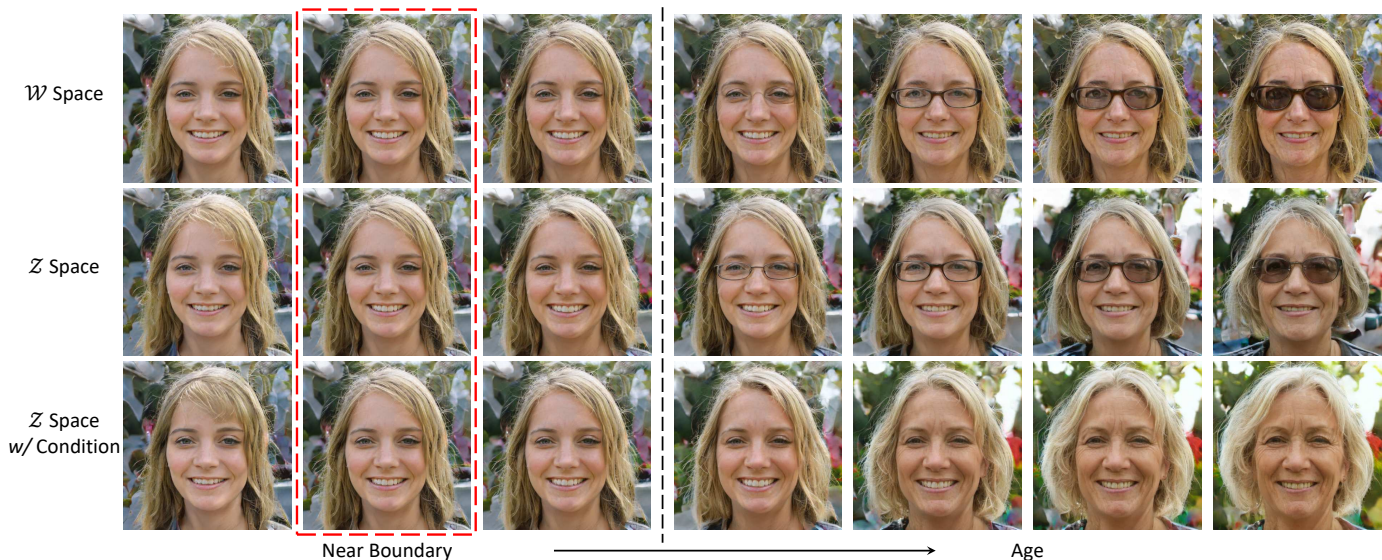


Fig. 11. **Conditional manipulation** analysis on StyleGAN [3] by taking age manipulation as an example. Images in red dashed boxes represent the original synthesis, while the others show the manipulation process. \mathcal{W} space is more disentangled than \mathcal{Z} space, especially for long-distance manipulation, but the entanglement in \mathcal{Z} space can be corrected by the proposed conditional manipulation. Such conditional manipulation operation is not applicable to \mathcal{W} space since \mathcal{W} space is somewhat “over-disentangled”.

subtracting its projection onto the gender direction from the age direction, resulting in a new direction. By moving latent codes along this projected direction, we can make sure the gender component is barely affected in the editing process (bottom row). Fig.10 shows a more complex case where we perform manipulation with multiple constraints. Taking “eyeglasses” attribute as an example, in the beginning, adding eyeglasses is entangled with changing both age and gender. But we manage to disentangle eyeglasses from age and gender by manually forcing the eyeglasses direction to be orthogonal to the other two. These two experiments demonstrate that our proposed conditional approach helps to achieve independent and precise attribute control.

4.3.3 StyleGAN

Disentanglement Analysis. We conduct similar analysis on the StyleGAN model trained in FF-HQ dataset [3]. As mentioned above, StyleGAN introduces a disentangled latent space \mathcal{W} beyond the original latent space \mathcal{Z} . Hence, we analyze the boundary correlation from both of these two spaces. Results are shown in Tab.2. Besides the conclusions

from PGGAN, we have three more observations. (i) “Smile” and “gender” are not correlated in CelebA-HQ (Tab.1(a)), but entangled in FF-HQ (Tab.2(a)). This phenomenon is also reflected in the synthesized data (Tab.2(b)). (ii) \mathcal{W} space (Tab.2(d)) is indeed more disentangled than \mathcal{Z} space (Tab.2(c)), as pointed out by Karras *et al.* [3]. In \mathcal{W} space, almost all attributes are orthogonal to each other. (iii) The boundary correlation from \mathcal{W} space no longer aligns with the semantic distribution from real data (Tab.2(a)). In other words, \mathcal{W} space may “over-disentangle” these semantics and encode some entanglement as a new “style”. For example, in the training data, men are more likely to wear eyeglasses than women. \mathcal{W} space may capture such information and learn “man with eyeglasses” as a coupled style.

Conditional Manipulation. We also evaluate the proposed conditional manipulation on the style-based generator to verify its generalization ability. In particular, given a sample, we manipulate its attribute from both \mathcal{Z} space and \mathcal{W} space, and then perform conditional manipulation in \mathcal{Z} space. Note that such conditional operation is *not* applicable

TABLE 3

Re-scoring analysis on the semantic manipulation achieved by InterFaceGAN. Each row shows the results by manipulating a particular attribute.

	(a) PGGAN [1].					(b) StyleGAN \mathcal{Z} space.					(c) StyleGAN \mathcal{W} space.				
	Pose	Smile	Age	Gender	Glasses	Pose	Smile	Age	Gender	Glasses	Pose	Smile	Age	Gender	Glasses
Pose	0.53	0.05	-0.09	-0.06	-0.01	0.47	0.03	-0.04	-0.01	-0.03	0.51	0.02	-0.06	0.01	-0.03
Smile	-0.01	0.60	0.03	-0.07	-0.01	-0.01	0.50	-0.17	-0.21	-0.07	0.00	0.50	-0.15	-0.09	-0.02
Age	-0.03	-0.03	0.50	0.35	0.08	0.00	-0.11	0.56	0.18	0.32	0.01	-0.02	0.54	0.03	0.20
Gender	-0.02	-0.07	0.20	0.59	0.08	0.01	-0.24	0.27	0.45	0.13	0.03	-0.07	0.01	0.45	0.05
Glasses	-0.01	0.00	0.19	0.37	0.24	-0.03	-0.06	0.37	0.24	0.40	0.00	0.01	0.09	0.03	0.41

to \mathcal{W} space. As shown in Tab.2(d), all boundaries are already orthogonal to each other. Projection barely changes the primal direction, which we call “over-disentanglement” problem. Fig.11 gives an example about the entanglement between “age” and “eyeglasses”. In Fig.11, manipulating from \mathcal{Z} space and \mathcal{W} space produces similar results when the latent code still locates near to the boundary. For long-distance manipulation, \mathcal{W} space (first row) shows superiority over \mathcal{Z} space, *e.g.*, hair length and face shape do not change in the first row. Even so, “age” and “eyeglasses” are still entangled with each other in both spaces. However, we can use the proposed conditional manipulation to decorrelate “eyeglasses” from “age” in \mathcal{Z} space (third row), resulting in more appealing results.

5 QUANTITATIVE ANALYSIS ON MANIPULATION

We show plenty of qualitative results in Sec.4.2 and Sec.4.3 to evaluate the controllable disentangled semantics identified by InterFaceGAN. In this part, we would like to quantitatively analyze the properties of the disentangled semantics and the editing process, including (i) whether the manipulation can indeed increase or decrease the attribute score, and how manipulating one attribute affects the scores of other attributes (Sec.5.1); (ii) how GANs learn the face representation layer by layer (Sec.5.2); and (iii) how the attribute manipulation affects the face identity (Sec.5.3).

5.1 Evaluating Editing Performance with Re-scoring

Re-scoring means to re-predict the attribute scores from the faces after manipulation. Then, we compute the score change by comparing with the scores before manipulation. This is used to verify whether the manipulation happens as what we want. For example, when we move the latent code towards “male” direction (*i.e.*, the positive direction of “gender” boundary), we would expect the “gender” score to increase. This metric can also be used to evaluate the disentanglement between different semantics. For example, if we want to see how “gender” and “age” correlate with each other, we can move the latent code along the “gender” boundary and see how the “age” score varies.

We use $2K$ synthesis for re-scoring analysis on PGGAN [1], StyleGAN [3] \mathcal{Z} space, and StyleGAN \mathcal{W} space, whose results are reported in Tab.3. We have three major conclusions. (i) InterFaceGAN is able to convincingly increase the target semantic scores by manipulating the appropriate attributes (see diagonal entries). (ii) Manipulating one attribute may affect the scores of other attributes. Taking PGGAN (Tab.3(a)) as an example, when manipulating

TABLE 4

Layer-wise analysis on the semantic manipulation achieved by InterFaceGAN using StyleGAN [3]. Each row shows the results by manipulating a particular attribute.

Layer	All	00-01	02-03	04-05	06-07	08-17
Pose	0.51	0.42	0.20	0.03	0.01	0.00
Smile	0.50	0.02	0.32	0.24	0.08	0.01
Age	0.54	0.09	0.20	0.23	0.19	0.04
Gender	0.45	0.05	0.44	0.10	0.02	0.00
Glasses	0.41	0.23	0.28	0.01	0.00	0.00

“age”, “gender” score also increases. This is consistent with the observation from Sec.4.3. Actually, we can treat this as another disentanglement measurement. Under this metric, we also see that \mathcal{W} space (Tab.3(c)) is more disentangled than \mathcal{Z} space (Tab.3(b)) in StyleGAN. (iii) This new metric is asymmetry. Taking PGGAN (Tab.3(a)) as an example, when we manipulate “age”, “eyeglasses” is barely affected. But when we manipulate “eyeglasses”, “age” score increase a lot. Same phenomenon also happens to “gender” and “eyeglasses”. This provides us more adequate information about the entanglement between the semantics learned in the latent representation.

5.2 Per-Layer Representation Learned by GANs

Different from the traditional generator, the style-based generator in StyleGAN [3] feeds the latent code to all convolutional layers. This enables us to study the per-layer representation. Given a particular boundary, we can use it to only modulate the latent codes that are fed into a subset of layers. In practice, we manually divide the 18 layers into 5 groups, *i.e.*, 00-01, 02-03, 04-05, 06-07, and 08-17. Then we conduct the same experiment as in re-scoring analysis.

Tab.4 and Fig.12 show the quantitative and qualitative results respectively. From Tab.4, we can see that “pose” is mostly controlled at layer 00-01, “smile” is controlled at layer 02-05, “age” is controlled at layer 02-07, “gender” is controlled at layer 02-03, and “eyeglasses” is controlled at layer 00-03. All attributes are barely affected by editing layer 08-17. Visualization results in Fig.12 also gives the same conclusion. It implies that GANs actually learn different representation at different layers. This provide us some insights into a better understanding of the learning mechanism of GANs.

5.3 Effect of Learned Semantics on Face Identity

Identity is very important for face analysis. Accordingly, we perform identity analysis to see how the identity



Fig. 12. **Layer-wise manipulation** results with StyleGAN [3]. On the top-left corner is the raw synthesis. Images in red dashed boxes highlight the best manipulation results except the all-layer manipulation.

TABLE 5
Identity discrepancy after the face manipulation using InterFaceGAN. Cosine distance is used as the evaluation metric. Larger number means lower similarity.

Layer	PGGAN \mathcal{Z} Space	StyleGAN $\tilde{\mathcal{Z}}$ Space	StyleGAN \mathcal{W} Space					
			All	00-01	02-03	04-05	06-07	08-17
Pose	0.48	0.41	0.46	0.39	0.28	0.07	0.03	0.01
Smile	0.24	0.31	0.21	0.04	0.20	0.10	0.04	0.01
Age	0.53	0.47	0.28	0.12	0.18	0.09	0.06	0.01
Gender	0.61	0.51	0.40	0.11	0.37	0.13	0.03	0.01
Glasses	0.55	0.49	0.37	0.21	0.29	0.09	0.06	0.01

information varies during the manipulation process of InterFaceGAN. Similar to the re-scoring analysis, we employ a face recognition engine to extract the identity features from the faces before and after semantic editing. Cosine distance is used as the metric to evaluate the discrepancy.

Tab.5 shows the results corresponding to different latent spaces from different models, from which we have following observations. (i) “Gender” affects the identity most and “smile” affects the identity least. Actually, this can be used to verify how sensitive the face identity is to a particular attribute. For example, “pose” and “eyeglasses” seem to also affect the identity a lot. This makes sense since large pose is always the obstacle in face recognition task and eyeglasses

are commonly used to disguise identity in real world. We may use InterFaceGAN to synthesize more hard samples to in turn improve the face recognition model. (ii) StyleGAN \mathcal{W} space best preserves the identity information due to its disentanglement property. That is because identity is much more complex than other semantics. A more disentangled representation is helpful in identity control. (iii) As for the layer-wise results, we can get similar conclusion to the layer-wise analysis in Sec.5.2.

6 REAL IMAGE MANIPULATION

In this section, we apply the semantics implicitly learned by GANs to real face editing. Since most of the GAN models

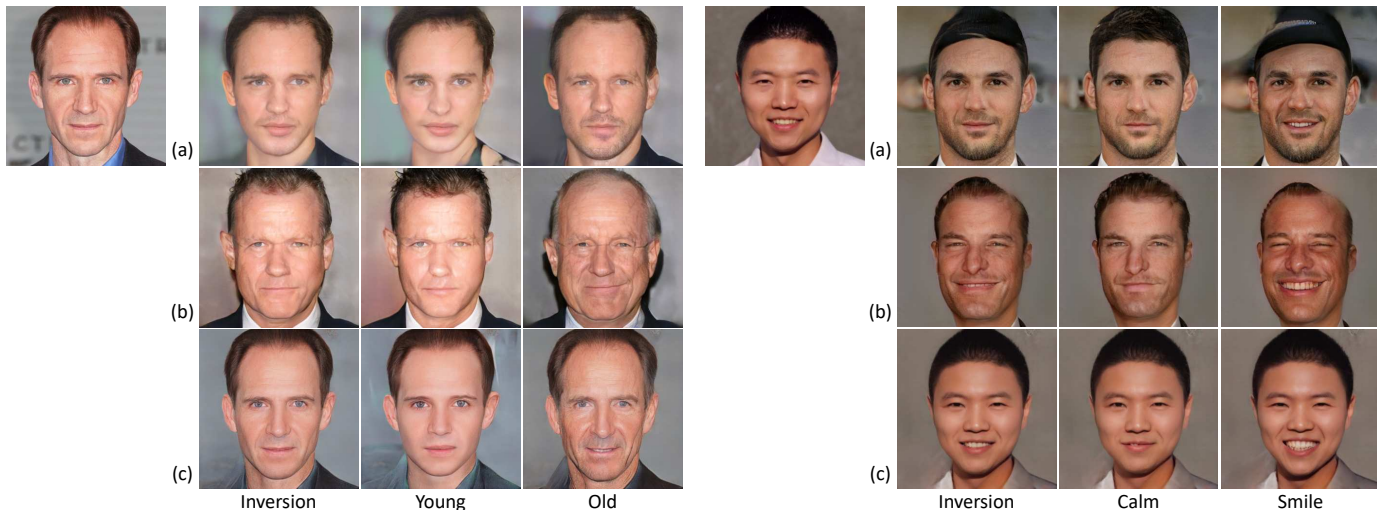


Fig. 13. **Manipulating real faces with GAN inversion**, using the pre-trained PGGAN [1] and StyleGAN [3]. Given an image to edit, we first invert it back to the latent code and then manipulate the latent code with InterFaceGAN. On the top-left corner is the input real face. From top to bottom: (a) PGGAN with optimization-based inversion method [45], (b) PGGAN with encoder-based inversion method [41], (c) StyleGAN with optimization-based inversion method [55].

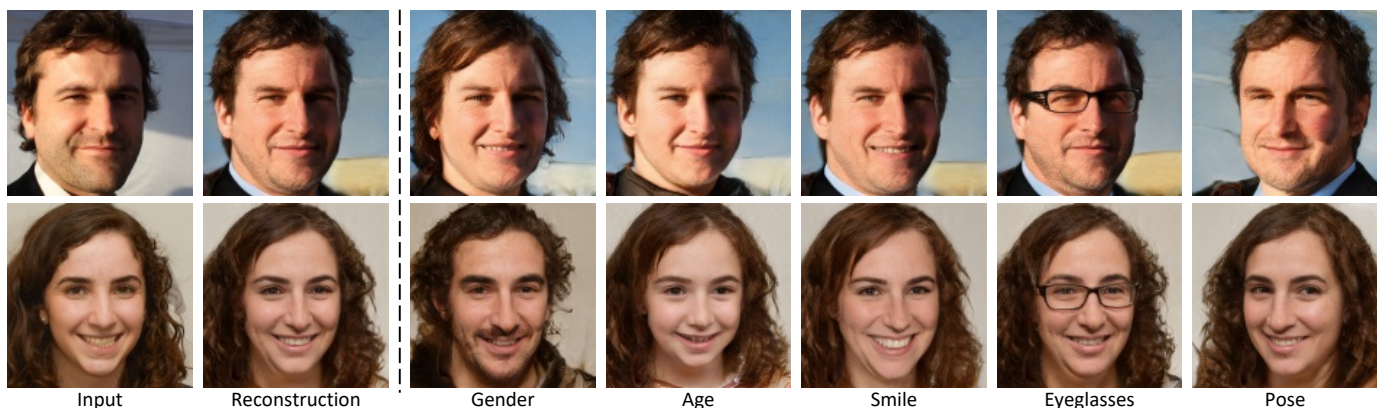


Fig. 14. **Manipulating real faces with encoder-decoder generative model, LIA** [50].

lack the inference function to deal with real images, we try two different approaches. One is based on GAN inversion, which inverts any given image to the latent code so that we can manipulate. The other uses InterFaceGAN to generate synthetic image pairs and trains additional feed-forward pixel-to-pixel models.

6.1 Combining GAN Inversion with InterFaceGAN

Recall that InterFaceGAN achieves semantic face editing by moving the latent code along a certain direction in the latent space. Accordingly, for real image editing, one straightforward way is to invert the target face back to a latent code. It turns out to be a non-trivial task because GANs do not fully capture all the modes as well as the diversity of the true distribution, which means it is extremely hard to perfectly recover any real image with a finitely dimensional latent code. To invert a pre-trained GAN model, there are two typical approaches. One is optimization-based approach, which directly optimizes the latent code with the fixed generator to minimize the pixel-wise reconstruction error [45], [55]. The other is encoder-based, where an extra encoder network is trained to learn the inverse mapping [41]. We tested the two baseline approaches on PGGAN [1] and StyleGAN [3].

Results are shown in Fig.13. We can tell that both optimization-based (first row) and encoder-based (second row) methods show poor performance when inverting PGGAN. This can be imputed to the strong discrepancy between training and testing data distributions. For example, the model tends to generate Western people even the input is an Easterner (see the right example in Fig.13). However, even unlike the inputs, the inverted images can still be semantically edited with InterFaceGAN. Compared to PGGAN, the results on StyleGAN (third row) are much better. Here, we treat the layer-wise styles (*i.e.*, w for all layers) as the optimization target following prior work [46], [47], [55]. Such over-parameterization significantly improves the inversion quality, and hence leads to better manipulation results. In this way, we are able to *turn conditional GANs, like StyleGAN, to controllable GANs*.

We also test InterFaceGAN on LIA [50], which is a generative model with encoder-decoder structure. It trains an encoder together with the generator and therefore has the inference ability. The manipulation result is shown in Fig.14 where we successfully edit the input faces with various attributes, like age and face pose. It suggests that the latent code in the encoder-decoder based generative models also supports semantic manipulation, demonstrating the

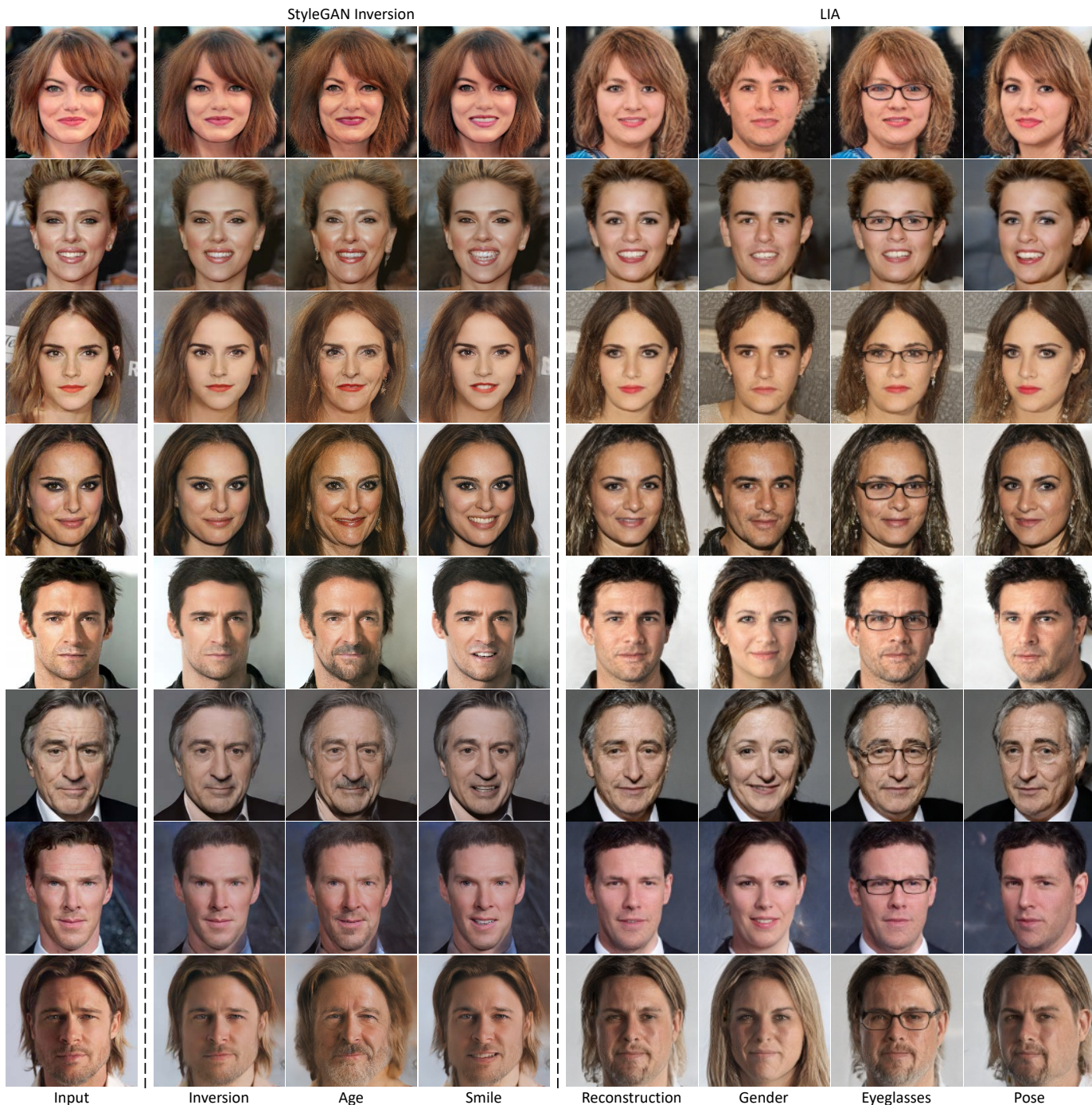


Fig. 15. **Real image manipulation** with StyleGAN inversion [55] and LIA [50].

generalization ability of InterFaceGAN. More results on StyleGAN inversion and LIA are shown in Fig.15. We can tell that the optimization-based method better recovers the input images and hence better preserves the identity information. But for both methods, the interpretable semantics inside the latent representation are capable of faithfully editing the corresponding facial attributes of the reconstructed face.

6.2 Training with Paired Synthetic Data Collected from InterFaceGAN

Another way to apply InterFaceGAN to real image editing is to train additional models. Different from existing face

manipulation models [6], [40], [64] that are trained on real dataset, we use InterFaceGAN to build synthetic dataset for training. There are two advantages: (i) With recent advancement, GANs are already able to produce high-quality image [3], [4], significantly narrowing the domain gap. (ii) With the strong manipulation capability of InterFaceGAN, we can easily create unlimited paired data, which is hard to collect in the real world. Taking eyeglasses editing as an example, we can sample numerous latent codes, move them along the “eyeglasses” direction, and re-score them to select the ones with highest score change. With paired data as input and supervision, we train pix2pixHD [59] to achieve face editing. However, pix2pixHD has its own shortcoming which is that

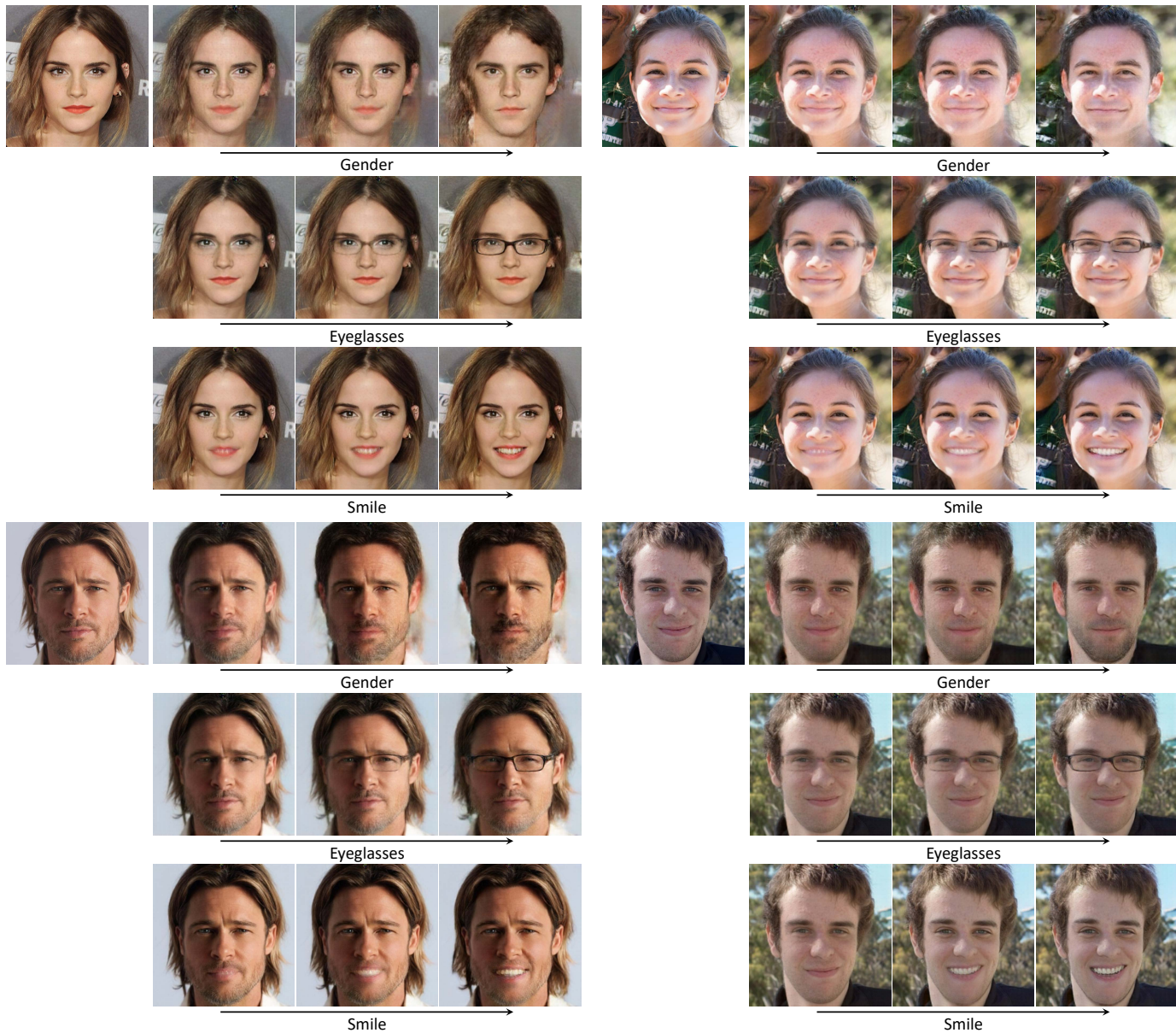


Fig. 16. **Real image manipulation by learning additional pix2pixHD models** [59] on synthetic dataset collected from InterFaceGAN. DNI [68] is used to get the gradually varying results. Note that the gender manipulation model only learns the mapping from female to male.

we cannot manipulate the attribute gradually [69]. To solve this problem, we introduce DNI [68] by first training an identical mapping network and then fine-tuning it for a particular attribute. We summarize the training pipeline as:

- 1) Prepare $10K$ synthetic pairs for each attribute.
- 2) Learn an identical pix2pixHD model.
- 3) Fine-tune the model to transfer a certain attribute.
- 4) Interpolate the model weights for gradual editing.

We choose “gender”, “eyeglasses”, and “smile” as the target attributes. Fig.16 shows the editing results. We can conclude that: (i) The pix2pixHD models trained on synthetic dataset can successfully manipulate the input face with respect to the target attribute. This suggests that the data generated by InterFaceGAN can well support model training, which may lead to more applications. (ii) For “gender” attribute, we only use female as the input and use male as the supervision. However, after the model training,

we can even use this model to add mustache onto male faces as shown in Fig.16 (bottom two examples). (iii) Following DNI [68], we interpolate the weight of the identical model and the weight of the fine-tuned model. By doing so, we can gradually manipulate the attributes of the input face, same as the inversion-based method described in Sec.6.1. The main advantage of learning additional feed-forward model is its fast inference speed. (iv) During the weight interpolation process, we find that “smile” attribute does not perform as well as “gender” and “eyeglasses”. That is because smiling is not a simple pixel-to-pixel translation task but requires the reasonable movement of lips. This is also the reason why pix2pixHD can not be applied to learning pose rotation, which requires larger movement. Accordingly, the major limitation of this kind of approach is that it can only transfer some easy-to-map semantics, such as “eyeglasses” and “age”.

7 DISCUSSION AND CONCLUSION

Interpreting the representation learned by GANs is vital for understanding the internal mechanism of the synthesis process, which yet remains less explored. In this work we provide some pilot results in this direction by taking face synthesis as an example. There are many future works to be done. As our visual world is far more complex than faces, looking into the generative models trained to synthesize other generic objects and scenes would be one of them. For example, for scene generation, besides learning the semantics for the entire image, the model should also learn to synthesize any individual object inside the scene as well as create a layout for different objects. From this point of view, we need a more general method to interpret other GAN models beyond faces. Even for face models, there are also some directions worth further exploring. On one hand, as we have already discussed in Sec.4.2, our method may fail for long-distance manipulation. This is restricted by the linear assumption. New adaptive method of changing the semantic boundary based on the latent code to manipulate would solve this problem. On the other hand, we use off-the-shelf classifiers as predictors to interpret the latent representation. This limits the semantics we can find since sometimes we may not have the proper classifiers or the attribute is not well defined or annotated. Hence, how to identify the semantics emerging from synthesizing images in an unsupervised learning manner would be future work as well.

To conclude, in this work we interpret the disentangled face representation learned by GANs and conduct a thorough study on the emerging facial semantics. By leveraging the semantic knowledge encoded in the latent space, we are able to realistically edit the attributes in face images. Conditional manipulation technique is further introduced to decorrelate different semantics for more precise control of facial attributes. Extensive experiments suggest that InterFaceGAN can also be applied to real image manipulation.

ACKNOWLEDGMENTS

This work is supported in part by the Early Career Scheme (ECS) through the Research Grants Council of Hong Kong under Grant No.24206219, in part by RSFS grant from CUHK Faculty of Engineering, and in part by SenseTime Collaborative Grant.

APPENDIX

PROOF

In this part, we provide detailed proof of *Property 2* in the main paper. Recall this property as follows.

Property 2 Given $\mathbf{n} \in \mathbb{R}^d$ with $\mathbf{n}^T \mathbf{n} = 1$, which defines a hyperplane, and a multivariate random variable $\mathbf{z} \sim \mathcal{N}(\mathbf{0}, \mathbf{I}_d)$, we have $\mathbb{P}(|\mathbf{n}^T \mathbf{z}| \leq 2\alpha \sqrt{\frac{d}{d-2}}) \geq (1 - 3e^{-cd})(1 - \frac{2}{\alpha} e^{-\alpha^2/2})$ for any $\alpha \geq 1$ and $d \geq 4$. Here $\mathbb{P}(\cdot)$ stands for probability and c is a fixed positive constant.

Proof.

Without loss of generality, we fix \mathbf{n} to be the first coordinate vector. Accordingly, it suffices to prove that

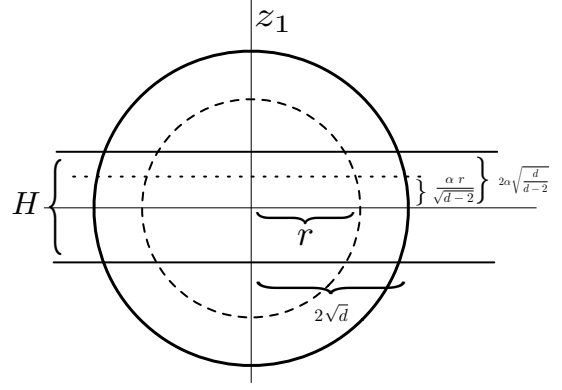


Fig. 17. Illustration of **Property 2**, which shows that most of the probability mass of high-dimensional Gaussian distribution lies in the thin slab near the “equator”.

$\mathbb{P}(|z_1| \leq 2\alpha \sqrt{\frac{d}{d-2}}) \geq (1 - 3e^{-cd})(1 - \frac{2}{\alpha} e^{-\alpha^2/2})$, where z_1 denotes the first entry of \mathbf{z} .

As shown in Fig.17, let H denote the set

$$\{\mathbf{z} \sim \mathbf{N}(\mathbf{0}, \mathbf{I}_d) : \|\mathbf{z}\|_2 \leq 2\sqrt{d}, |z_1| \leq 2\alpha \sqrt{\frac{d}{d-2}}\},$$

where $\|\cdot\|_2$ stands for the l_2 norm. Obviously, we have $\mathbb{P}(H) \leq \mathbb{P}(|z_1| \leq 2\alpha \sqrt{\frac{d}{d-2}})$. Now, we will show $\mathbb{P}(H) \geq (1 - 3e^{-cd})(1 - \frac{2}{\alpha} e^{-\alpha^2/2})$

Considering the random variable $R = \|\mathbf{z}\|_2$, with cumulative distribution function $F(R \leq r)$ and density function $f(r)$, we have

$$\begin{aligned} \mathbb{P}(H) &= \mathbb{P}(|z_1| \leq 2\alpha \sqrt{\frac{d}{d-2}} | R \leq 2\sqrt{d}) \mathbb{P}(R \leq 2\sqrt{d}) \\ &= \int_0^{2\sqrt{d}} \mathbb{P}(|z_1| \leq 2\alpha \sqrt{\frac{d}{d-2}} | R = r) f(r) dr. \end{aligned}$$

According to *Theorem 1* below, when $r \leq 2\sqrt{d}$, we have

$$\begin{aligned} \mathbb{P}(H) &= \int_0^{2\sqrt{d}} \mathbb{P}(|z_1| \leq 2\alpha \sqrt{\frac{d}{d-2}} | R = r) f(r) dr \\ &= \int_0^{2\sqrt{d}} \mathbb{P}(|z_1| \leq \frac{2\sqrt{d}}{r} \frac{\alpha}{\sqrt{d-2}} | R = 1) f(r) dr \\ &\geq \int_0^{2\sqrt{d}} \mathbb{P}(|z_1| \leq \frac{\alpha}{\sqrt{d-2}} | R = 1) f(r) dr \\ &\geq \int_0^{2\sqrt{d}} (1 - \frac{2}{\alpha} e^{-\alpha^2/2}) f(r) dr \\ &= (1 - \frac{2}{\alpha} e^{-\alpha^2/2}) \int_0^{2\sqrt{d}} f(r) dr \\ &= (1 - \frac{2}{\alpha} e^{-\alpha^2/2}) \mathbb{P}(0 \leq R \leq 2\sqrt{d}). \end{aligned}$$

Then, according to *Theorem 2* below, by setting $\beta = \sqrt{d}$, we have

$$\begin{aligned} \mathbb{P}(H) &= (1 - \frac{2}{\alpha} e^{-\alpha^2/2}) \mathbb{P}(0 \leq R \leq 2\sqrt{d}) \\ &\geq (1 - \frac{2}{\alpha} e^{-\alpha^2/2}) (1 - 3e^{-cd}). \end{aligned}$$

Q.E.D.

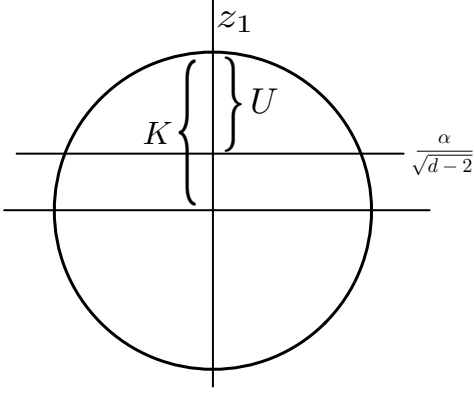


Fig. 18. Diagram for **Theorem 1**.

Theorem 1 Given a unit spherical $\{\mathbf{z} \in \mathbb{R}^d : \|\mathbf{z}\|_2 = 1\}$, we have $P(|z_1| \leq \frac{\alpha}{\sqrt{d-2}}) \geq 1 - \frac{2}{\alpha} e^{-\alpha^2/2}$ for any $\alpha \geq 1$ and $d \geq 4$.

Proof.

By symmetry, we just prove the case where $z_1 \geq 0$. Also, we only consider about the case where $\frac{\alpha}{\sqrt{d-2}} \leq 1$.

Let U denote the set $\{\mathbf{z} \in \mathbb{R}^d : \|\mathbf{z}\|_2 = 1, z_1 \geq \frac{\alpha}{\sqrt{d-2}}\}$, and K denote the set $\{\mathbf{z} \in \mathbb{R}^d : \|\mathbf{z}\|_2 = 1, z_1 \geq 0\}$. It suffices to prove that the surface of U area and the surface of K area in Fig.18 satisfy

$$\frac{\text{surf}(U)}{\text{surf}(K)} \leq \frac{2}{\alpha} e^{-\alpha^2/2},$$

where $\text{surf}(\cdot)$ stands for the surface area of a high dimensional geometry. Let $A(d)$ denote the surface area of a d -dimensional unit-radius ball. Then, we have

$$\begin{aligned} \text{surf}(U) &= \int_{\frac{\alpha}{\sqrt{d-2}}}^1 (1 - z_1^2)^{\frac{d-2}{2}} A(d-1) dz_1 \\ &\leq \int_{\frac{\alpha}{\sqrt{d-2}}}^1 e^{-\frac{d-2}{2} z_1^2} A(d-1) dz_1 \\ &\leq \int_{\frac{\alpha}{\sqrt{d-2}}}^1 \frac{z_1 \sqrt{d-2}}{\alpha} e^{-\frac{d-2}{2} z_1^2} A(d-1) dz_1 \\ &\leq \int_{\frac{\alpha}{\sqrt{d-2}}}^{\infty} \frac{z_1 \sqrt{d-2}}{\alpha} e^{-\frac{d-2}{2} z_1^2} A(d-1) dz_1 \\ &= \frac{A(d-1)}{\alpha \sqrt{d-2}} e^{-\alpha^2/2}. \end{aligned}$$

Similarly, we have

$$\begin{aligned} \text{surf}(K) &= \int_0^1 (1 - z_1^2)^{\frac{d-2}{2}} A(d-1) dz_1 \\ &\geq \int_0^{\frac{1}{\sqrt{d-2}}} (1 - z_1^2)^{\frac{d-2}{2}} A(d-1) dz_1 \\ &\geq \frac{1}{\sqrt{d-2}} \left(1 - \frac{1}{d-2}\right)^{\frac{d-2}{2}} A(d-1). \end{aligned}$$

Considering the fact that $(1-x)^a \geq 1-ax$ for any $a \geq 1$ and $0 \leq x \leq 1$, we have

$$\begin{aligned} \text{surf}(K) &\geq \frac{1}{\sqrt{d-2}} \left(1 - \frac{1}{d-2}\right)^{\frac{d-2}{2}} A(d-1) \\ &\geq \frac{1}{\sqrt{d-2}} \left(1 - \frac{1}{d-2} \frac{d-2}{2}\right) A(d-1) \end{aligned}$$

$$= \frac{A(d-1)}{2\sqrt{d-2}}.$$

Accordingly,

$$\frac{\text{surf}(U)}{\text{surf}(K)} \leq \frac{\frac{A(d-1)}{\alpha \sqrt{d-2}} e^{-\alpha^2/2}}{\frac{A(d-1)}{2\sqrt{d-2}}} = \frac{2}{\alpha} e^{-\alpha^2/2}.$$

Q.E.D.

Theorem 2 (Gaussian Annulus Theorem [70]) For a d -dimensional spherical Gaussian with unit variance in each direction, for any $\beta \leq \sqrt{d}$, all but at most $3e^{-c\beta^2}$ of the probability mass lies within the annulus $\sqrt{d} - \beta \leq \|\mathbf{z}\|_2 \leq \sqrt{d} + \beta$, where c is a fixed positive constant.

That is to say, given $\mathbf{z} \sim \mathbf{N}(\mathbf{0}, \mathbf{I}_d)$, $\beta \leq \sqrt{d}$, and a constant $c > 0$, we have

$$P(\sqrt{d} - \beta \leq \|\mathbf{z}\|_2 \leq \sqrt{d} + \beta) \geq (1 - 3e^{-c\beta^2}).$$

REFERENCES

- [1] T. Karras, T. Aila, S. Laine, and J. Lehtinen, "Progressive growing of GANs for improved quality, stability, and variation," in *ICLR*, 2018.
- [2] I. Goodfellow, J. Pouget-Abadie, M. Mirza, B. Xu, D. Warde-Farley, S. Ozair, A. Courville, and Y. Bengio, "Generative adversarial nets," in *NeurIPS*, 2014.
- [3] T. Karras, S. Laine, and T. Aila, "A style-based generator architecture for generative adversarial networks," in *CVPR*, 2019.
- [4] T. Karras, S. Laine, M. Aittala, J. Hellsten, J. Lehtinen, and T. Aila, "Analyzing and improving the image quality of stylegan," *arXiv preprint arXiv:1912.04958*, 2019.
- [5] Y. Shen, J. Gu, X. Tang, and B. Zhou, "Interpreting the latent space of gans for semantic face editing," in *CVPR*, 2020.
- [6] G. Lample, N. Zeghidour, N. Usunier, A. Bordes, L. Denoyer, and M. Ranzato, "Fader networks: Manipulating images by sliding attributes," in *NeurIPS*, 2017.
- [7] D. Bau, H. Strobel, W. Peebles, J. Wulff, B. Zhou, J.-Y. Zhu, and A. Torralba, "Semantic photo manipulation with a generative image prior," *SIGGRAPH*, 2019.
- [8] C. Ledig, L. Theis, F. Huszár, J. Caballero, A. Cunningham, A. Acosta, A. Aitken, A. Tejani, J. Totz, Z. Wang *et al.*, "Photo-realistic single image super-resolution using a generative adversarial network," in *CVPR*, 2017.
- [9] X. Wang, K. Yu, S. Wu, J. Gu, Y. Liu, C. Dong, Y. Qiao, and C. Change Loy, "Esrgan: Enhanced super-resolution generative adversarial networks," in *ECCV Workshop*, 2018.
- [10] R. A. Yeh, C. Chen, T. Yan Lim, A. G. Schwing, M. Hasegawa-Johnson, and M. N. Do, "Semantic image inpainting with deep generative models," in *CVPR*, 2017.
- [11] J. Yu, Z. Lin, J. Yang, X. Shen, X. Lu, and T. S. Huang, "Free-form image inpainting with gated convolution," in *ICCV*, 2019.
- [12] T.-C. Wang, M.-Y. Liu, J.-Y. Zhu, G. Liu, A. Tao, J. Kautz, and B. Catanzaro, "Video-to-video synthesis," in *NeurIPS*, 2018.
- [13] T.-C. Wang, M.-Y. Liu, A. Tao, G. Liu, J. Kautz, and B. Catanzaro, "Few-shot video-to-video synthesis," *arXiv preprint arXiv:1910.12713*, 2019.
- [14] M. Arjovsky, S. Chintala, and L. Bottou, "Wasserstein generative adversarial networks," in *ICML*, 2017.
- [15] I. Gulrajani, F. Ahmed, M. Arjovsky, V. Dumoulin, and A. C. Courville, "Improved training of wasserstein gans," in *NeurIPS*, 2017.
- [16] T. Miyato, T. Kataoka, M. Koyama, and Y. Yoshida, "Spectral normalization for generative adversarial networks," in *ICLR*, 2018.
- [17] H. Zhang, I. Goodfellow, D. Metaxas, and A. Odena, "Self-attention generative adversarial networks," in *ICML*, 2019.
- [18] D. Berthelot, T. Schumm, and L. Metz, "Began: Boundary equilibrium generative adversarial networks," *arXiv preprint arXiv:1703.10717*, 2017.
- [19] A. Brock, J. Donahue, and K. Simonyan, "Large scale GAN training for high fidelity natural image synthesis," in *ICLR*, 2019.
- [20] N. Chen, A. Klushyn, R. Kurle, X. Jiang, J. Bayer, and P. van der Smagt, "Metrics for deep generative models," in *AISTAT*, 2018.

- [21] G. Arvanitidis, L. K. Hansen, and S. Hauberg, "Latent space oddity: on the curvature of deep generative models," in *ICLR*, 2018.
- [22] L. Kuhnel, T. Fletcher, S. Joshi, and S. Sommer, "Latent space non-linear statistics," *arXiv preprint arXiv:1805.07632*, 2018.
- [23] S. Laine, "Feature-based metrics for exploring the latent space of generative models," in *ICLR Workshop*, 2018.
- [24] H. Shao, A. Kumar, and P. Thomas Fletcher, "The riemannian geometry of deep generative models," in *CVPR Workshop*, 2018.
- [25] P. Bojanowski, A. Joulin, D. Lopez-Pas, and A. Szlam, "Optimizing the latent space of generative networks," in *ICML*, 2018.
- [26] D. Bau, J.-Y. Zhu, H. Strobel, B. Zhou, J. B. Tenenbaum, W. T. Freeman, and A. Torralba, "Gan dissection: Visualizing and understanding generative adversarial networks," in *ICLR*, 2019.
- [27] A. Radford, L. Metz, and S. Chintala, "Unsupervised representation learning with deep convolutional generative adversarial networks," in *ICLR*, 2016.
- [28] P. Upchurch, J. Gardner, G. Pleiss, R. Pless, N. Snaveley, K. Bala, and K. Weinberger, "Deep feature interpolation for image content changes," in *CVPR*, 2017.
- [29] L. Goetschalckx, A. Andonian, A. Oliva, and P. Isola, "Ganalyze: Toward visual definitions of cognitive image properties," in *ICCV*, 2019.
- [30] A. Jahanian, L. Chai, and P. Isola, "On the "steerability" of generative adversarial networks," in *ICLR*, 2020.
- [31] C. Yang, Y. Shen, and B. Zhou, "Semantic hierarchy emerges in deep generative representations for scene synthesis," *arXiv preprint arXiv:1911.09267*, 2019.
- [32] A. Odena, C. Olah, and J. Shlens, "Conditional image synthesis with auxiliary classifier gans," in *ICML*, 2017.
- [33] X. Chen, Y. Duan, R. Houthoofd, J. Schulman, I. Sutskever, and P. Abbeel, "Infogan: Interpretable representation learning by information maximizing generative adversarial nets," in *NeurIPS*, 2016.
- [34] L. Tran, X. Yin, and X. Liu, "Disentangled representation learning gan for pose-invariant face recognition," in *CVPR*, 2017.
- [35] X. Yin, X. Yu, K. Sohn, X. Liu, and M. Chandraker, "Towards large-pose face frontalization in the wild," in *ICCV*, 2017.
- [36] J. Bao, D. Chen, F. Wen, H. Li, and G. Hua, "Towards open-set identity preserving face synthesis," in *CVPR*, 2018.
- [37] T. Xiao, J. Hong, and J. Ma, "Elegant: Exchanging latent encodings with gan for transferring multiple face attributes," in *ECCV*, 2018.
- [38] Y. Shen, B. Zhou, P. Luo, and X. Tang, "Facefeat-gan: a two-stage approach for identity-preserving face synthesis," *arXiv preprint arXiv:1812.01288*, 2018.
- [39] C. Donahue, A. Balsubramani, J. McAuley, and Z. C. Lipton, "Semantically decomposing the latent spaces of generative adversarial networks," in *ICLR*, 2018.
- [40] Y. Shen, P. Luo, J. Yan, X. Wang, and X. Tang, "Faceid-gan: Learning a symmetry three-player gan for identity-preserving face synthesis," in *CVPR*, 2018.
- [41] J.-Y. Zhu, P. Krähenbühl, E. Shechtman, and A. A. Efros, "Generative visual manipulation on the natural image manifold," in *ECCV*, 2016.
- [42] G. Perarnau, J. Van De Weijer, B. Raducanu, and J. M. Álvarez, "Invertible conditional gans for image editing," in *NeurIPS Workshop*, 2016.
- [43] Z. C. Lipton and S. Tripathi, "Precise recovery of latent vectors from generative adversarial networks," in *ICLR Workshop*, 2017.
- [44] A. Creswell and A. A. Bharath, "Inverting the generator of a generative adversarial network," *TNNLS*, 2018.
- [45] F. Ma, U. Ayaz, and S. Karaman, "Invertibility of convolutional generative networks from partial measurements," in *NeurIPS*, 2018.
- [46] A. Rameen, Q. Yipeng, and W. Peter, "Image2stylegan: How to embed images into the stylegan latent space?" in *ICCV*, 2019.
- [47] R. Abdal, Y. Qin, and P. Wonka, "Image2stylegan++: How to edit the embedded images?" *arXiv preprint arXiv:1911.11544*, 2019.
- [48] V. Dumoulin, I. Belghazi, B. Poole, O. Mastropietro, A. Lamb, M. Arjovsky, and A. Courville, "Adversarially learned inference," in *ICLR*, 2017.
- [49] J. Donahue, P. Krähenbühl, and T. Darrell, "Adversarial feature learning," in *ICLR*, 2017.
- [50] J. Zhu, D. Zhao, and B. Zhang, "Lia: Latently invertible autoencoder with adversarial learning," *arXiv preprint arXiv:1906.08090*, 2019.
- [51] D. Bau, J.-Y. Zhu, J. Wulff, W. Peebles, H. Strobel, B. Zhou, and A. Torralba, "Seeing what a gan cannot generate," in *ICCV*, 2019.
- [52] —, "Inverting layers of a large generator," in *ICLR Workshop*, 2019.
- [53] J. Gu, Y. Shen, and B. Zhou, "Image processing using multi-code gan prior," in *CVPR*, 2020.
- [54] X. Pan, X. Zhan, B. Dai, D. Lin, C. C. Loy, and P. Luo, "Exploiting deep generative prior for versatile image restoration and manipulation," *arXiv preprint arXiv:2003.13659*, 2020.
- [55] J. Zhu, Y. Shen, D. Zhao, and B. Zhou, "In-domain gan inversion for real image editing," *arXiv preprint arXiv:2004.00049*, 2020.
- [56] L. Karacan, Z. Akata, A. Erdem, and E. Erdem, "Learning to generate images of outdoor scenes from attributes and semantic layouts," *arXiv preprint arXiv:1612.00215*, 2016.
- [57] T. Park, M.-Y. Liu, T.-C. Wang, and J.-Y. Zhu, "Semantic image synthesis with spatially-adaptive normalization," in *CVPR*, 2019.
- [58] P. Isola, J.-Y. Zhu, T. Zhou, and A. A. Efros, "Image-to-image translation with conditional adversarial networks," in *CVPR*, 2017.
- [59] T.-C. Wang, M.-Y. Liu, J.-Y. Zhu, A. Tao, J. Kautz, and B. Catanzaro, "High-resolution image synthesis and semantic manipulation with conditional gans," in *CVPR*, 2018.
- [60] M.-Y. Liu, T. Breuel, and J. Kautz, "Unsupervised image-to-image translation networks," in *NeurIPS*, 2017.
- [61] J.-Y. Zhu, T. Park, P. Isola, and A. A. Efros, "Unpaired image-to-image translation using cycle-consistent adversarial networks," in *ICCV*, 2017.
- [62] X. Huang, M.-Y. Liu, S. Belongie, and J. Kautz, "Multimodal unsupervised image-to-image translation," in *ECCV*, 2018.
- [63] J.-Y. Zhu, R. Zhang, D. Pathak, T. Darrell, A. A. Efros, O. Wang, and E. Shechtman, "Toward multimodal image-to-image translation," in *NeurIPS*, 2017.
- [64] Y. Choi, M. Choi, M. Kim, J.-W. Ha, S. Kim, and J. Choo, "Stargan: Unified generative adversarial networks for multi-domain image-to-image translation," in *CVPR*, 2018.
- [65] Y. Choi, Y. Uh, J. Yoo, and J.-W. Ha, "Stargan v2: Diverse image synthesis for multiple domains," in *CVPR*, 2020.
- [66] Z. Liu, P. Luo, X. Wang, and X. Tang, "Deep learning face attributes in the wild," in *ICCV*, 2015.
- [67] K. He, X. Zhang, S. Ren, and J. Sun, "Deep residual learning for image recognition," in *CVPR*, 2016.
- [68] X. Wang, K. Yu, C. Dong, X. Tang, and C. C. Loy, "Deep network interpolation for continuous imagery effect transition," in *CVPR*, 2019.
- [69] Y. Viazovetskyi, V. Ivashkin, and E. Kashin, "Stylegan2 distillation for feed-forward image manipulation," *arXiv preprint arXiv:2003.03581*, 2020.
- [70] A. Blum, J. Hopcroft, and R. Kannan, *Foundations of data science*. Cambridge University Press, 2020.